

The STIX imaging problem: methods and first results

Paolo Massa, MIDA, Department of Mathematics, University of Genoa

February 3, 2022



n | w

Outline

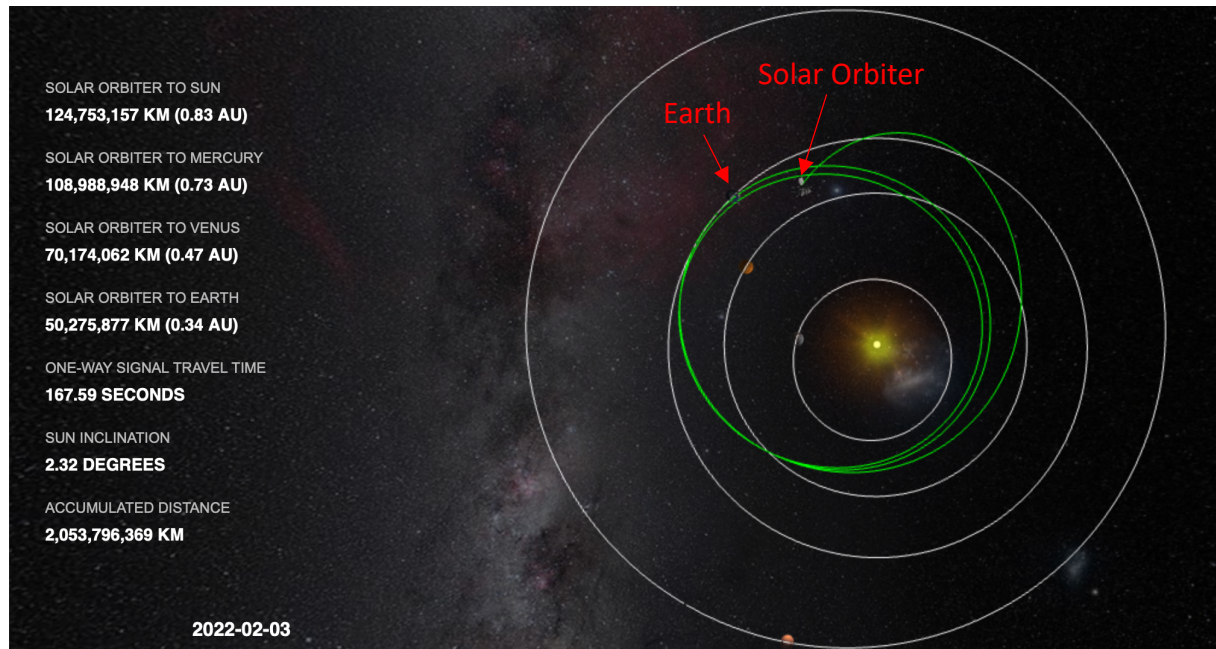
- STIX imaging concept
- Overview of the methods for image reconstruction from STIX data
- Results obtained on several events recorded in May 2021

STIX in Solar Orbiter

Solar Orbiter: ESA mission launched on February 10, 2020



(credits: ESA website)



(<https://solarorbiter.esac.esa.int/where/>)

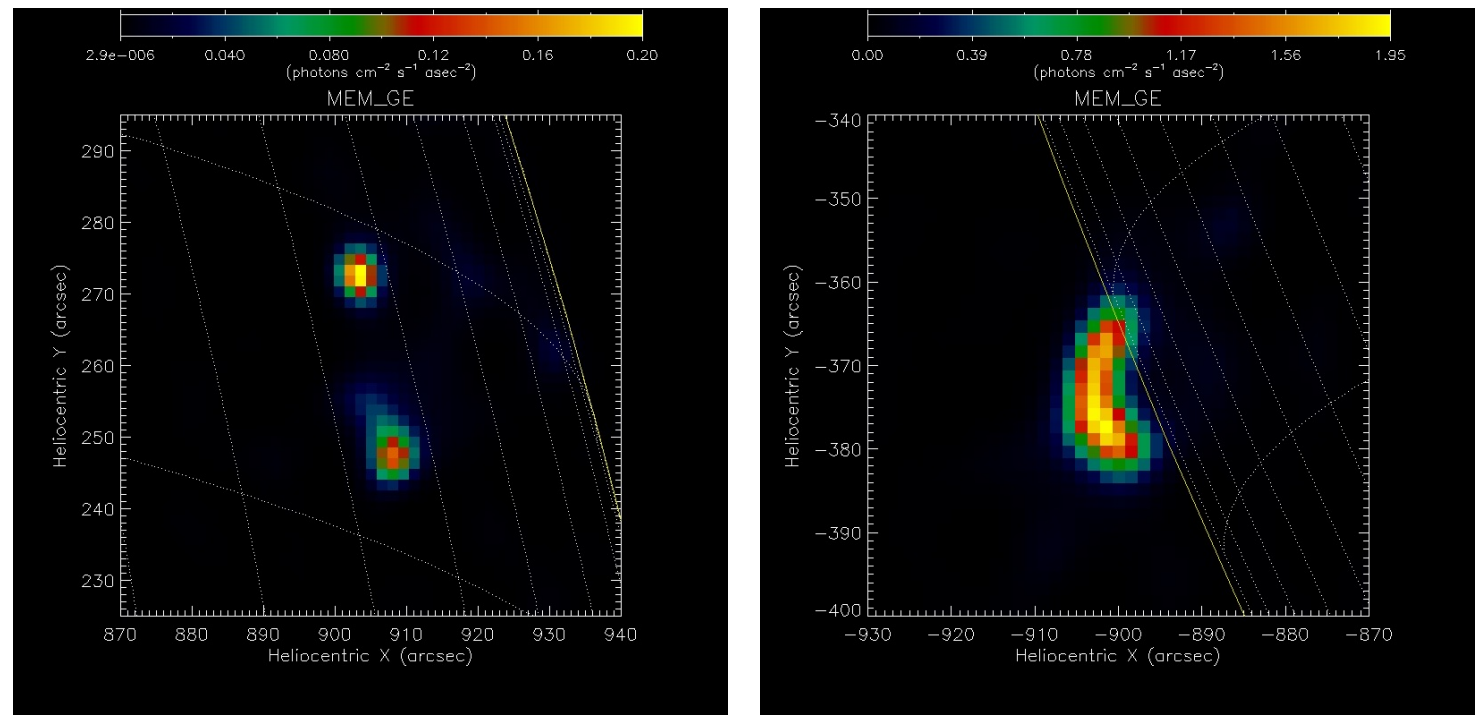
The STIX instrument

- **STIX:** Spectrometer/Telescope for Imaging X-rays
- **Scientific goal:** provide information on electrons accelerated during a solar flare
- **How:** by measuring X-ray photons emitted by bremsstrahlung

The STIX instrument

- **STIX:** Spectrometer/Telescope for Imaging X-rays
- **Scientific goal:** provide information on electrons accelerated during a solar flare
- **How:** by measuring X-ray photons emitted by bremsstrahlung

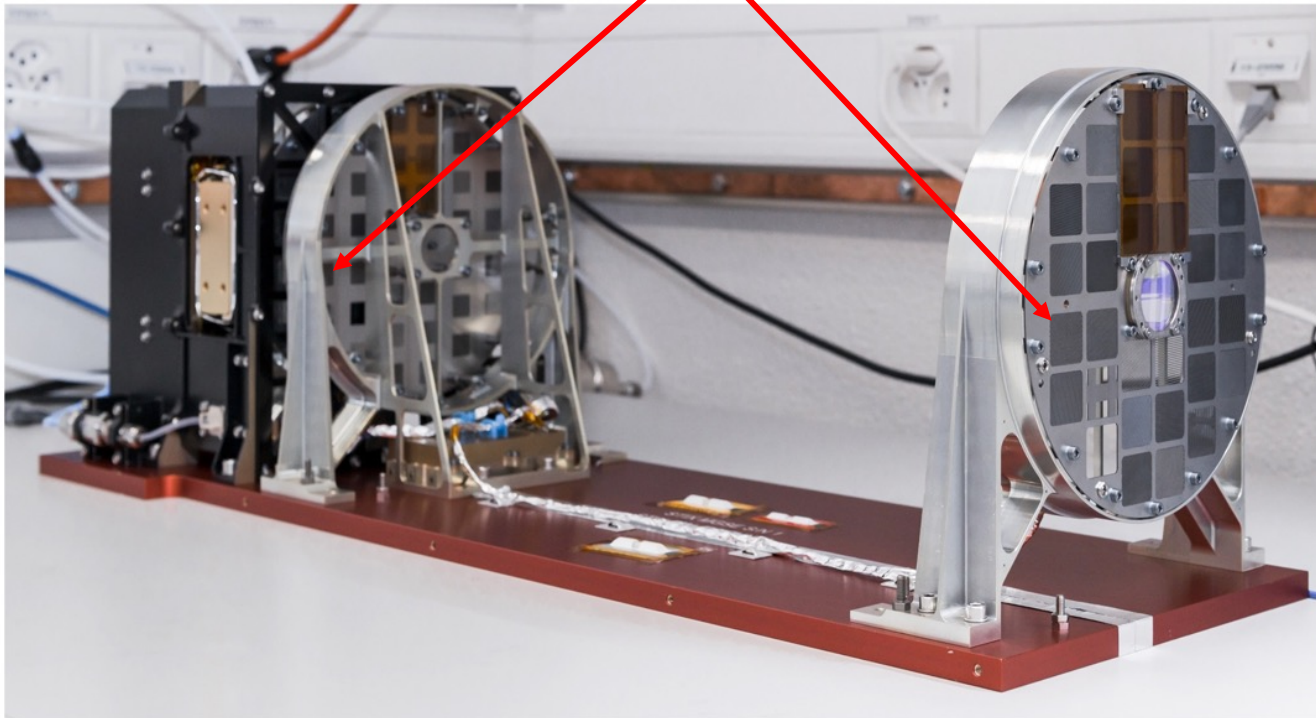
Images of solar flare X-ray emissions (from RHESSI data)



STIX imaging objective: reconstruct the image of the flaring X-ray emission form indirect measurements

The STIX instrument

Sub-collimator = front grid + rear grid + detector



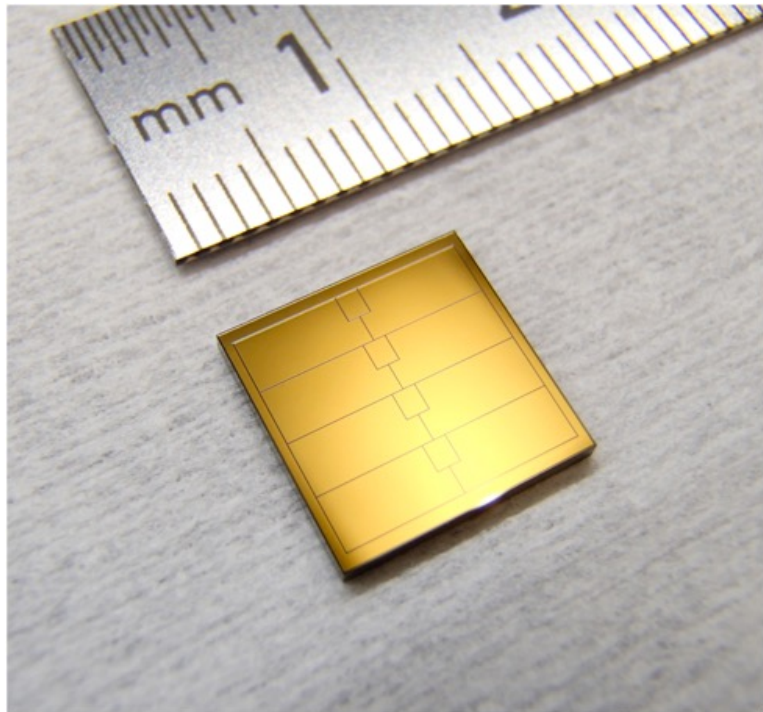
(Krucker et al., 2020)

- Bi-grid imaging system
- STIX consists of 32 subcollimators:
 - 30 are used for imaging
 - Coarse Flare Locator
 - Background monitor

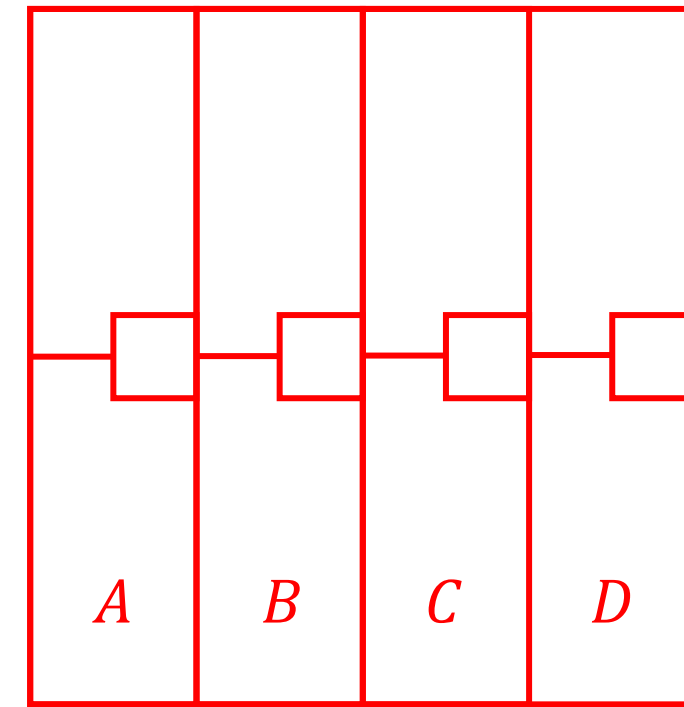
The STIX instrument

STIX Cadmium-Telluride detector

(Meuris et al. 2015)

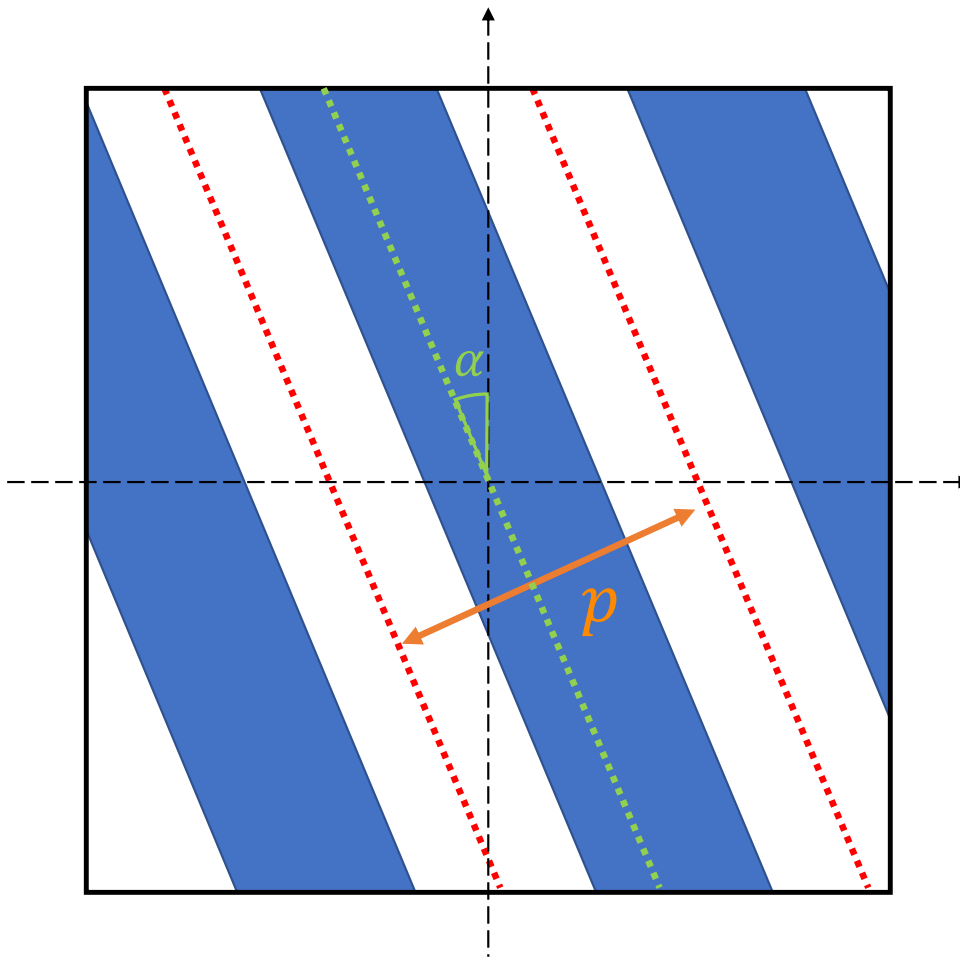


Krucker et al., 2020



A, B, C and D: number of counts
recorded by the detector pixels

The STIX instrument

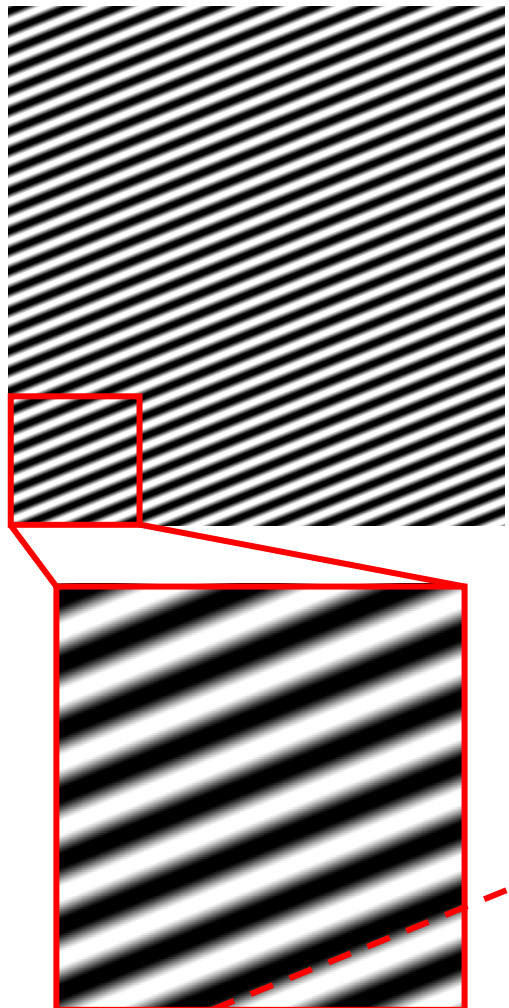


Grid parameters:

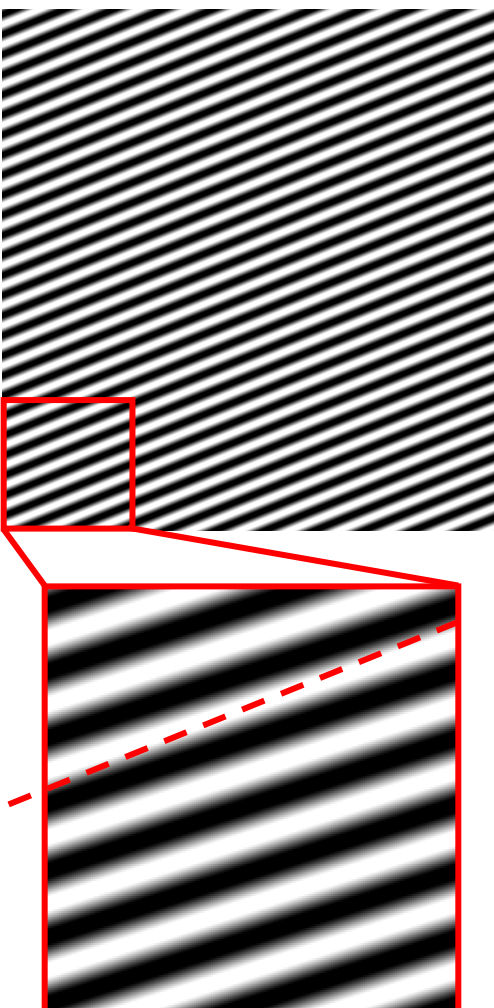
- α : orientation angle
- p : pitch = distance
between two consecutive
slit centers

The STIX imaging concept

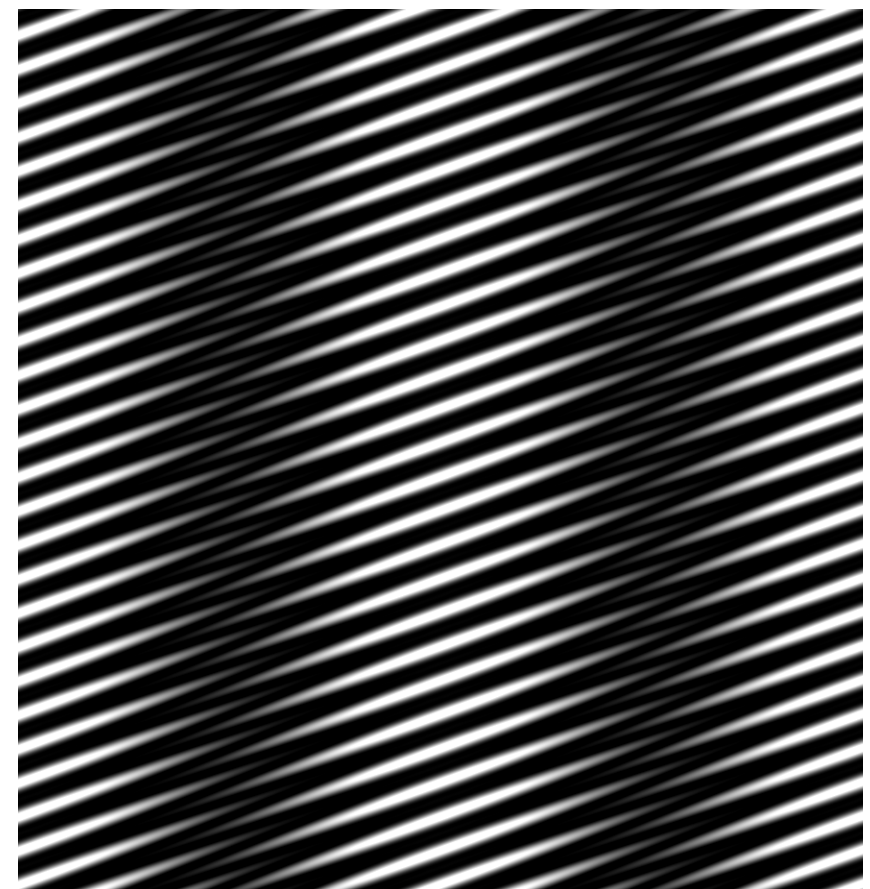
Front grid



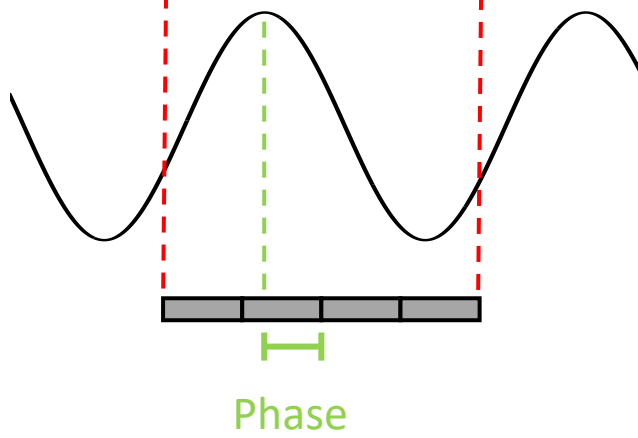
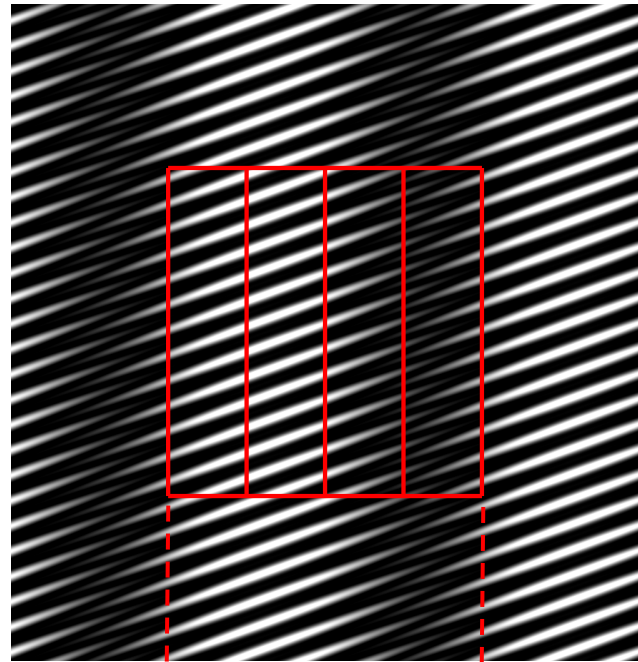
Rear grid



Moiré pattern



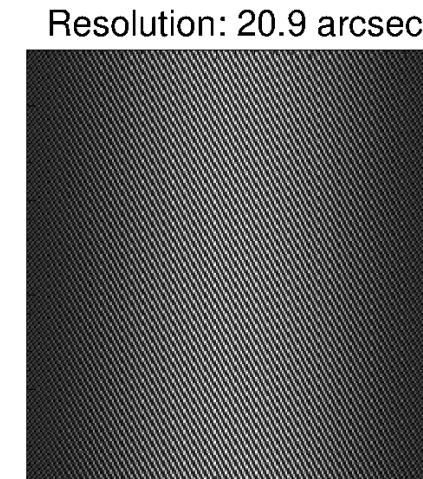
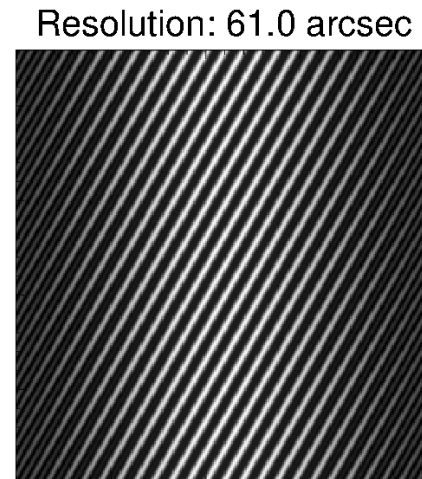
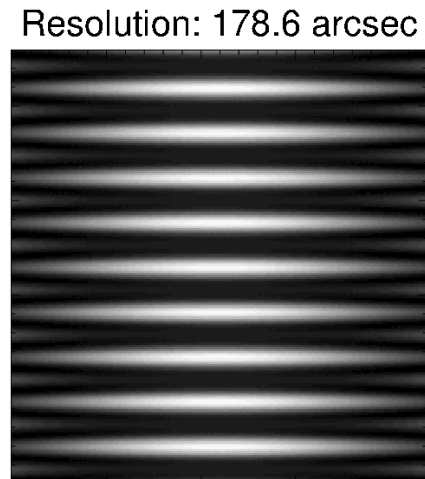
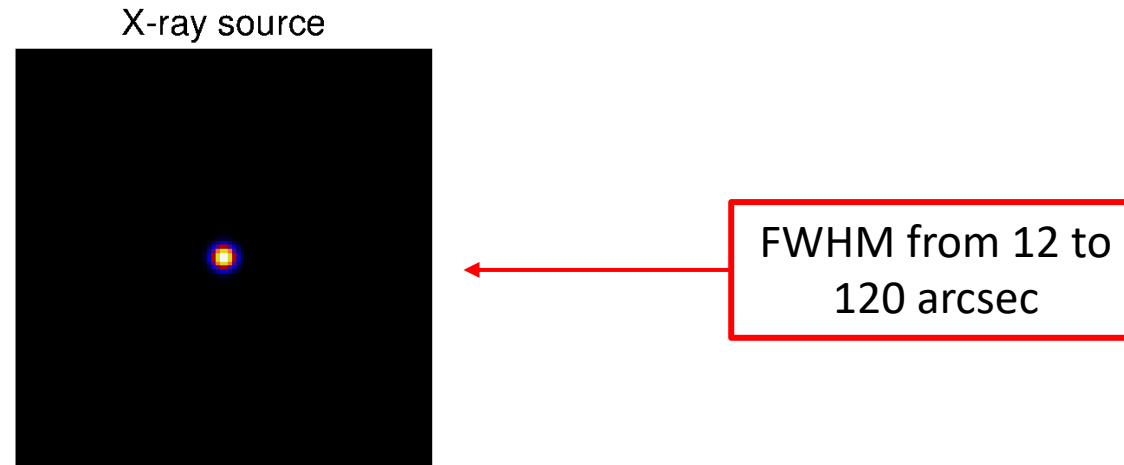
The STIX imaging concept



- Moiré pattern: sinusoidal wave with period equal to the detector width
- Amplitude and phase of the pattern → amplitude and phase of a Fourier component of the photon flux (**visibility**)

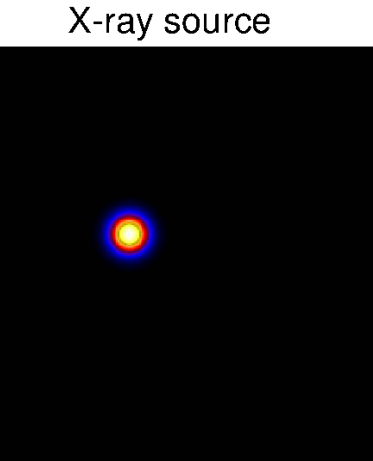
The STIX imaging concept

The amplitude of a Moiré pattern is sensitive to the source size and shape

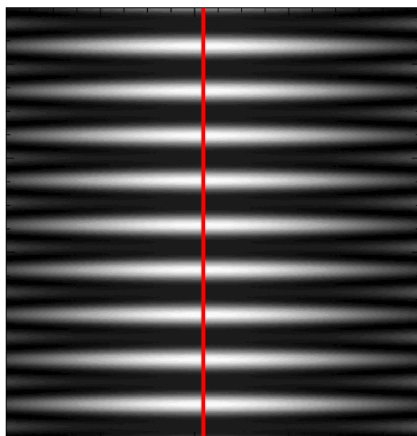


The STIX imaging concept

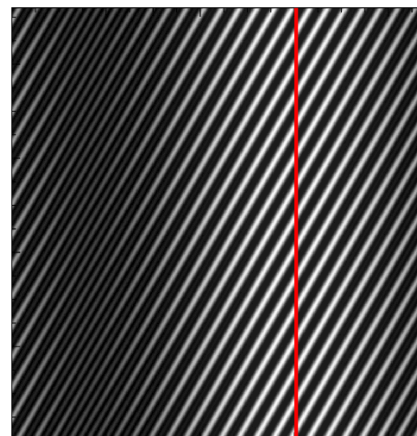
The phase of a Moiré pattern is sensitive to the source location



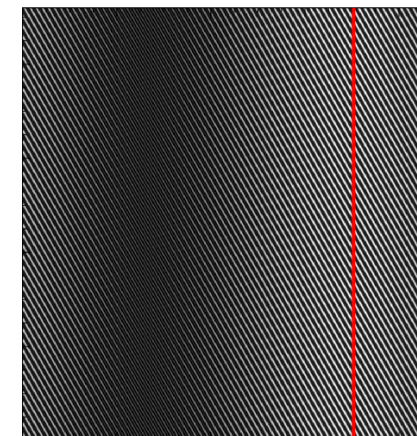
Resolution: 178.6 arcsec



Resolution: 61.0 arcsec



Resolution: 20.9 arcsec

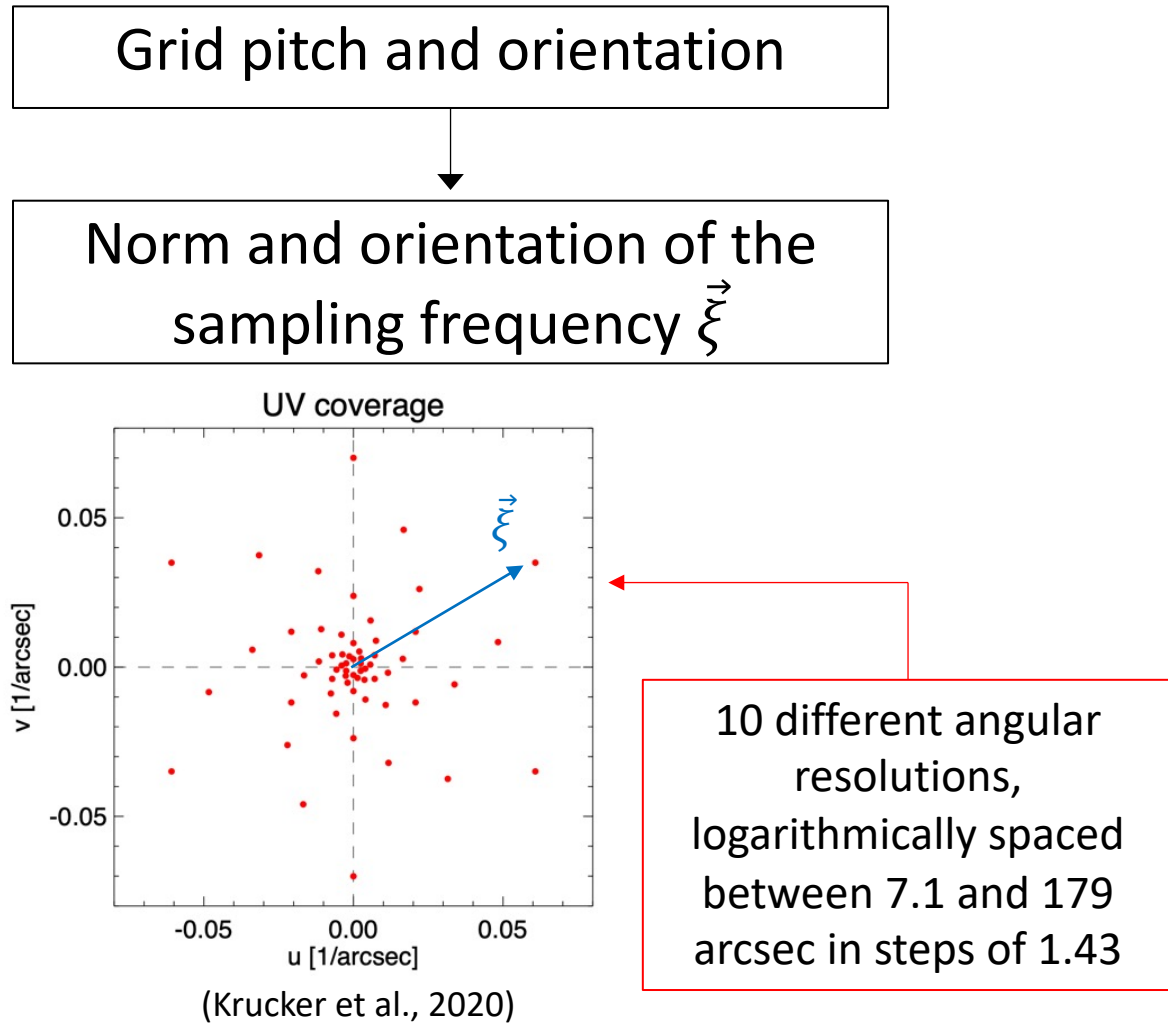


The STIX imaging concept

Each sub-collimator measures a visibility value

The STIX imaging concept

Each sub-collimator measures a visibility value



The STIX imaging concept

Each sub-collimator measures a visibility value

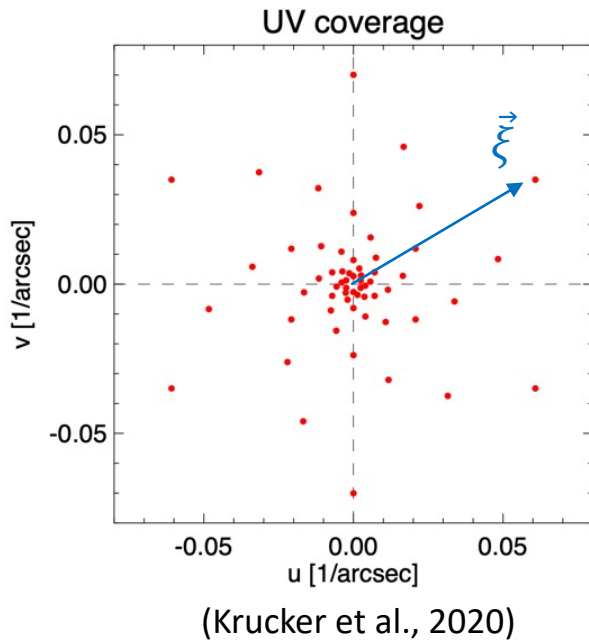
Grid pitch and orientation

Count measurements A, B, C, D

Norm and orientation of the sampling frequency ξ

Amplitude and phase of the visibility:

- $|V| \propto \sqrt{(C - A)^2 + (D - B)^2}$
- $\phi = \text{atan} \left(\frac{D-B}{C-A} \right) + 45^\circ + \phi_{calib}$



10 different angular resolutions,
logarithmically spaced
between 7.1 and 179 arcsec in steps of 1.43

The STIX imaging concept

Each sub-collimator measures a visibility value

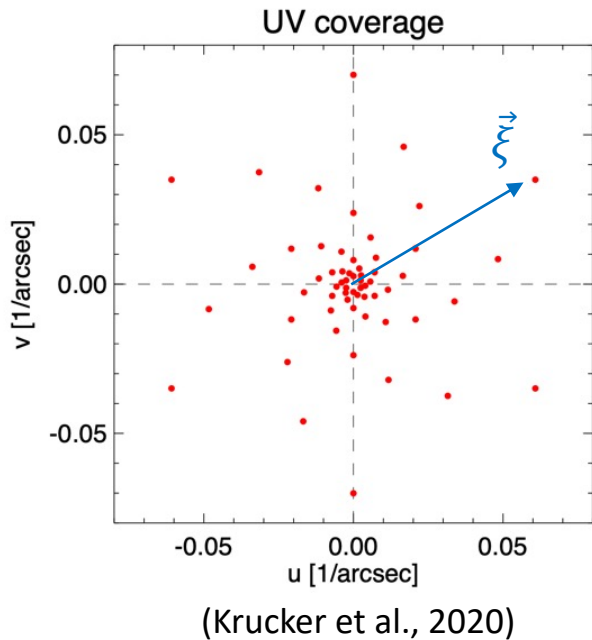
Grid pitch and orientation

Count measurements A, B, C, D

Norm and orientation of the sampling frequency ξ

Amplitude and phase of the visibility:

- $|V| \propto \sqrt{(C - A)^2 + (D - B)^2}$
- $\phi = \text{atan} \left(\frac{D-B}{C-A} \right) + 45^\circ + \phi_{\text{calib}}$



10 different angular resolutions,
logarithmically spaced
between 7.1 and 179 arcsec in steps of 1.43

**The data measured by STIX
are 30 visibilities**

STIX vs RHESSI

RHESSI: Reuven Ramaty High Energy Solar Spectroscopic Imager (Lin et al., 2002), NASA telescope working from 2002 to 2018



Similarities: both hard X-ray Fourier imagers

Differences:

	STIX	RHESSI
Imaging concept	Moiré patterns	Rotating Modulation Collimators
Number of visibilities	30	$\sim 10^2$
Orbit	Around the Sun (up to 0.28 AU)	Around the Earth
Finest angular resolution	7.1 arcsec	2.3 arcsec
Time resolution	< 1 sec	~ 2 sec
Energy range	4-150 keV	3 keV to 17 MeV
Energy resolution	1 keV (below 16 keV)	1 keV at 3 keV
Image placement accuracy	4 arcsec	< 1 arcsec

Image reconstruction problem

Image reconstruction problem for STIX:

$$F\phi = V$$

Where:

- ϕ is the image to reconstruct
- F is the Fourier transform
- V is the complex array of visibilities

This problem is analogous to the RHESSI one: we can use the same algorithms

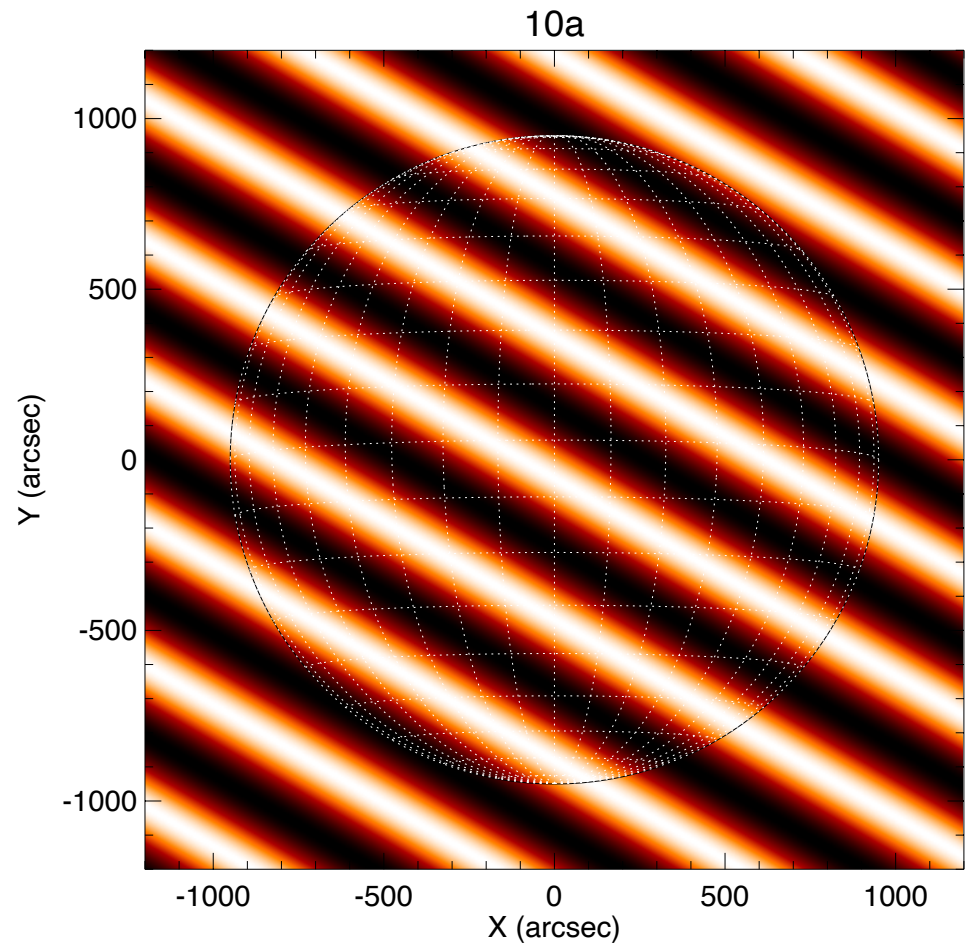
Back projection (Mertz et al., 1986)

- Direct Fourier inversion of the visibilities
- The Back Projection of a single visibility is a sinusoidal wave

$$\phi(x, y) = A \sin(2\pi(xu + yv) - \theta)$$

where

- A is the visibility amplitude
- θ is the visibility phase
- (u, v) is the angular frequency sampled by the sub-collimator



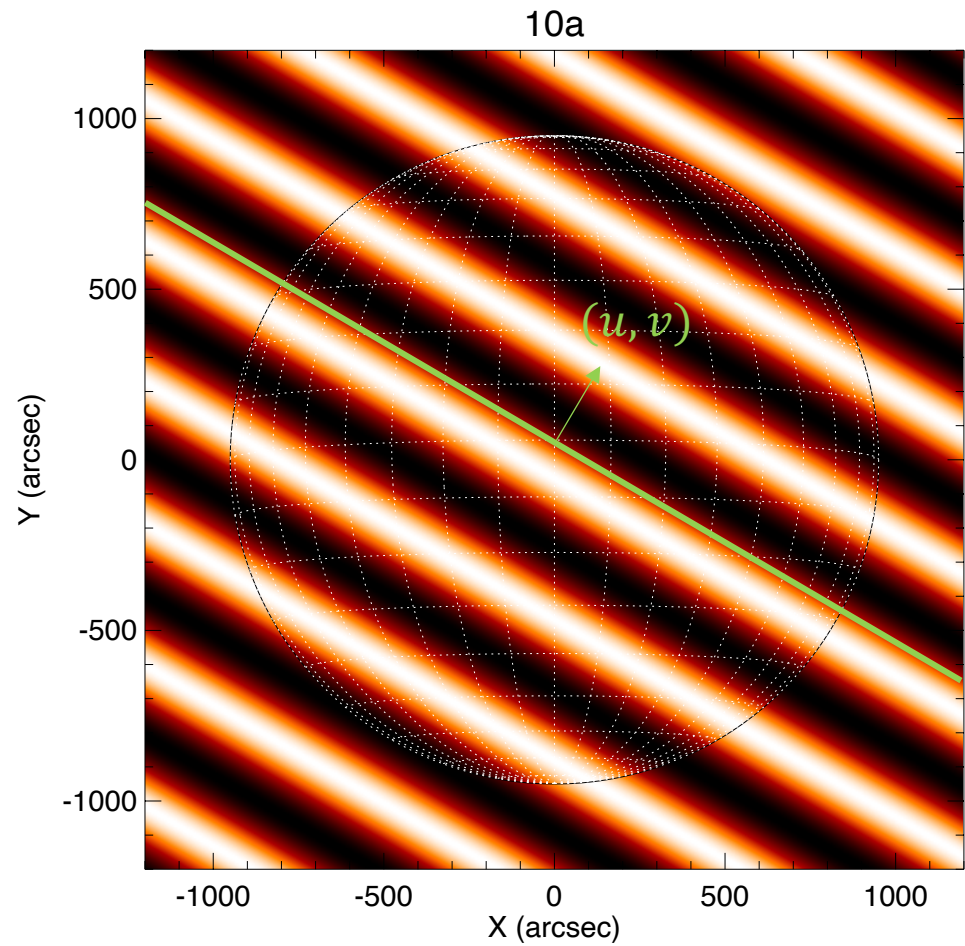
Back projection (Mertz et al., 1986)

- Direct Fourier inversion of the visibilities
- The Back Projection of a single visibility is a sinusoidal wave

$$\phi(x, y) = A \sin(2\pi(xu + yv) - \theta)$$

where

- A is the visibility amplitude
- θ is the visibility phase
- (u, v) is the angular frequency sampled by the sub-collimator



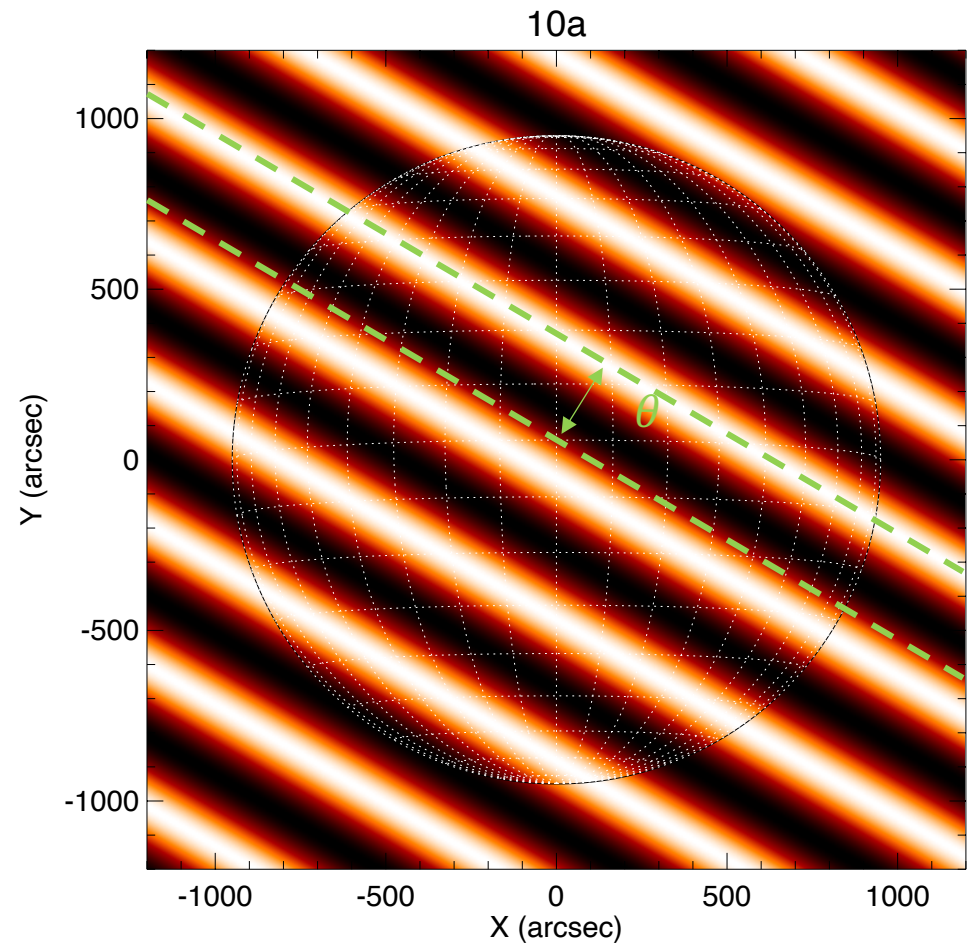
Back projection (Mertz et al., 1986)

- Direct Fourier inversion of the visibilities
- The Back Projection of a single visibility is a sinusoidal wave

$$\phi(x, y) = A \sin(2\pi(xu + yv) - \theta)$$

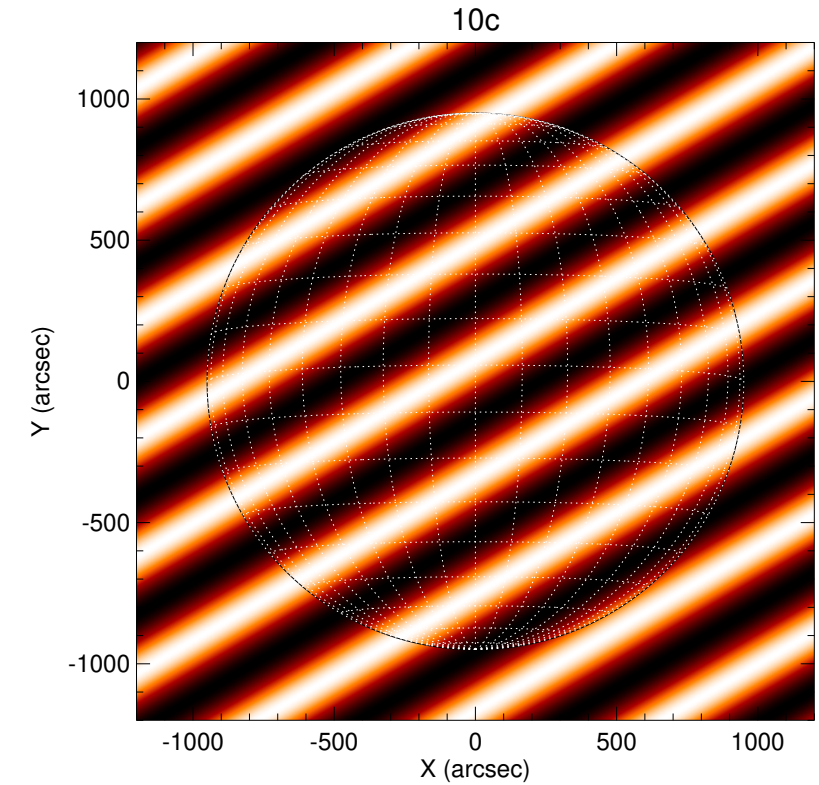
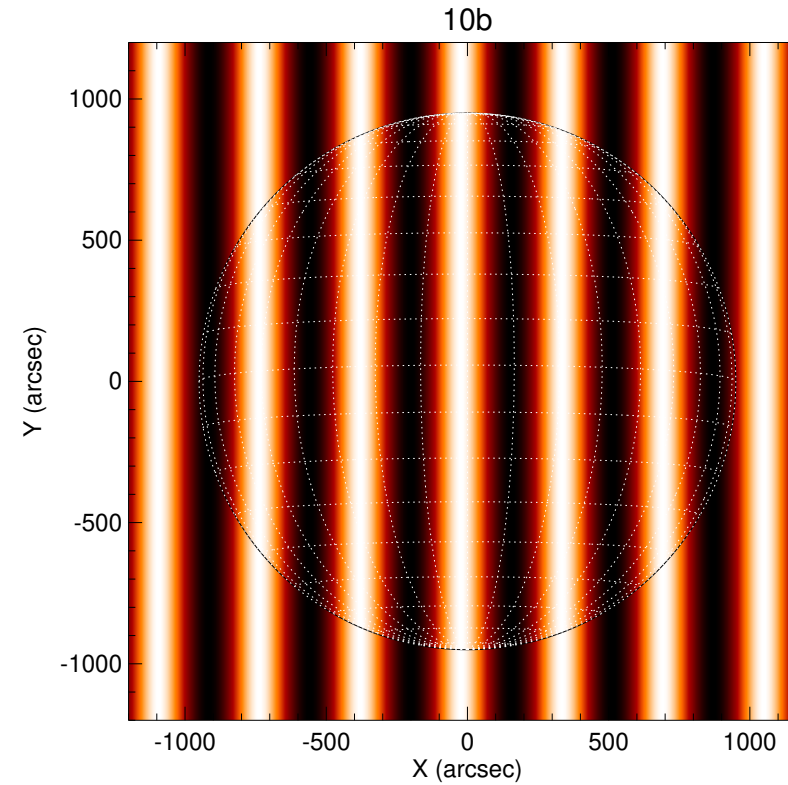
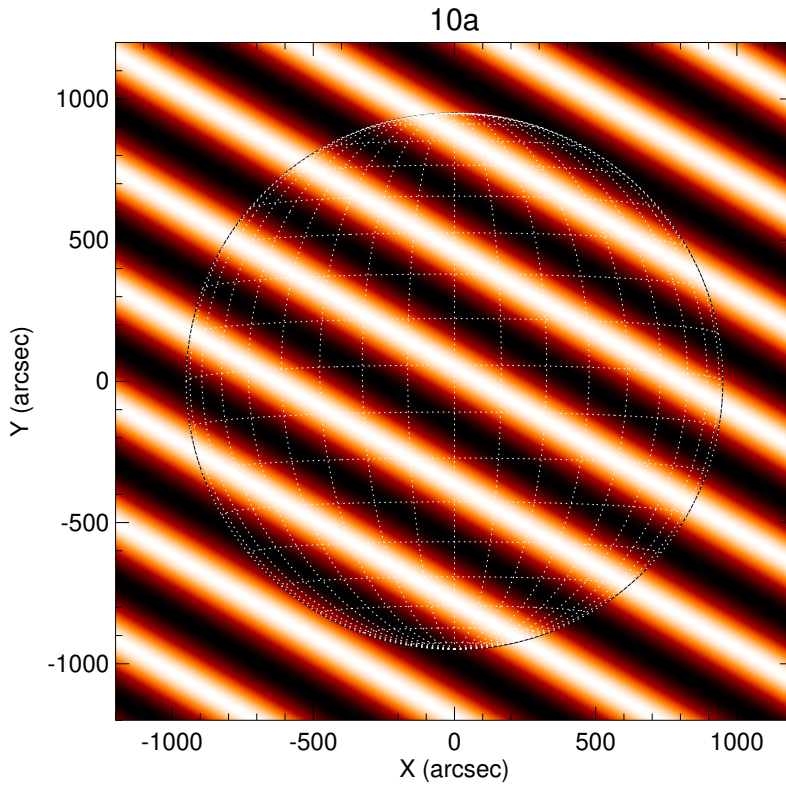
where

- A is the visibility amplitude
- θ is the visibility phase
- (u, v) is the angular frequency sampled by the sub-collimator



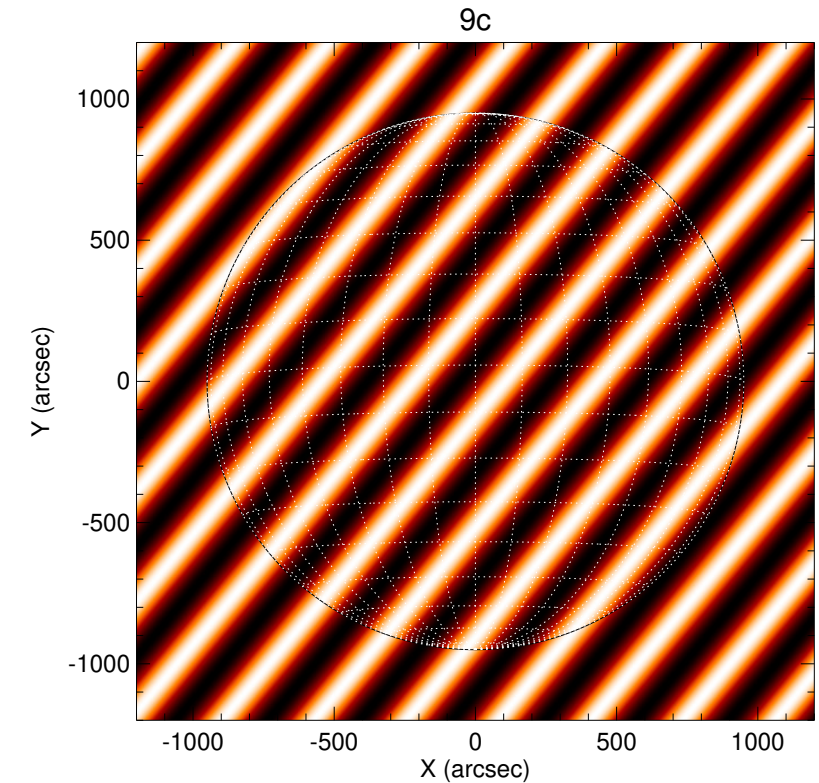
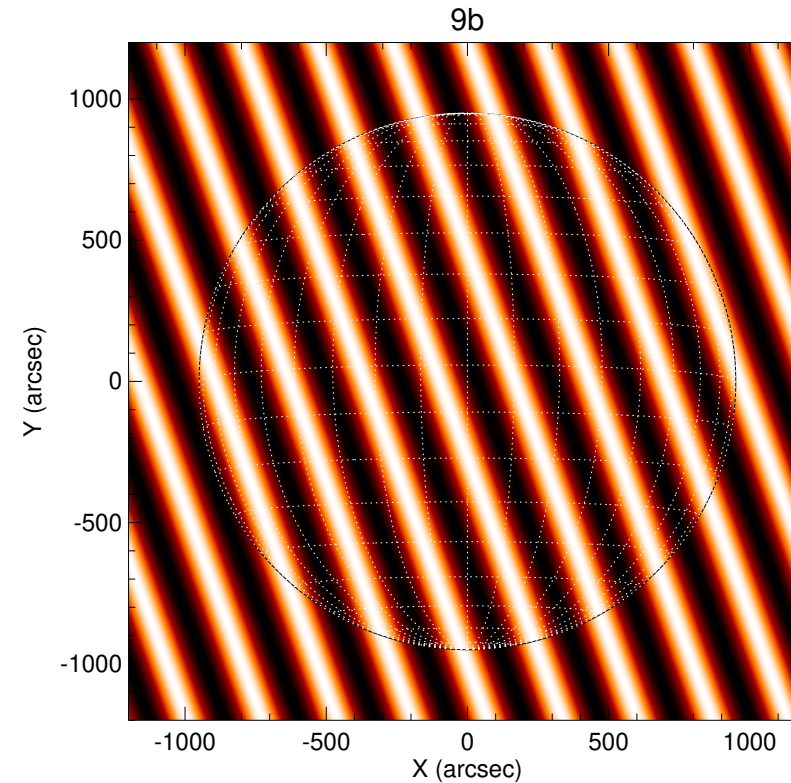
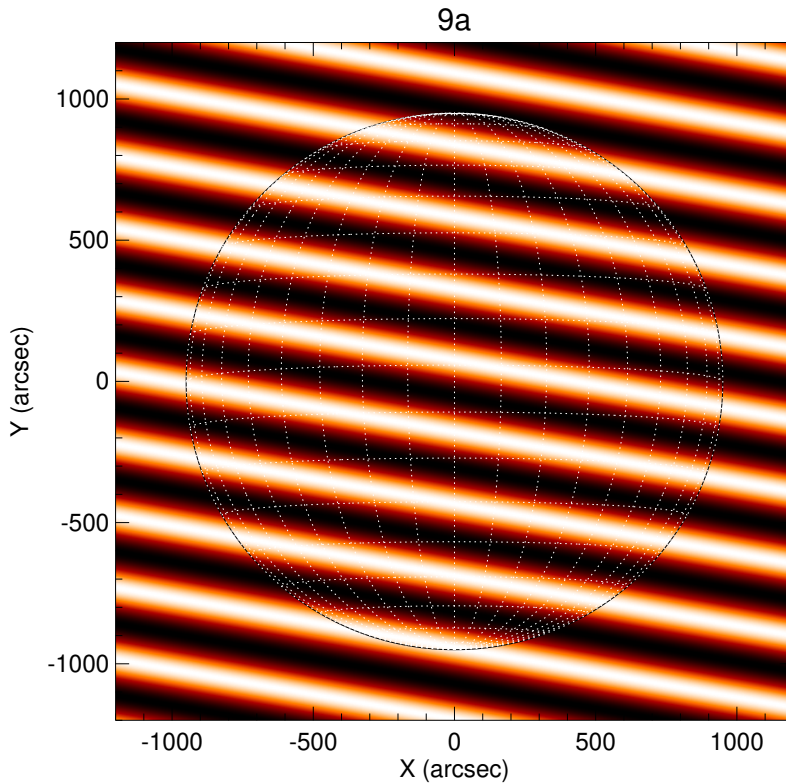
Back projection (Mertz et al., 1986)

Detectors with the same resolution produce waves with same period but different orientation



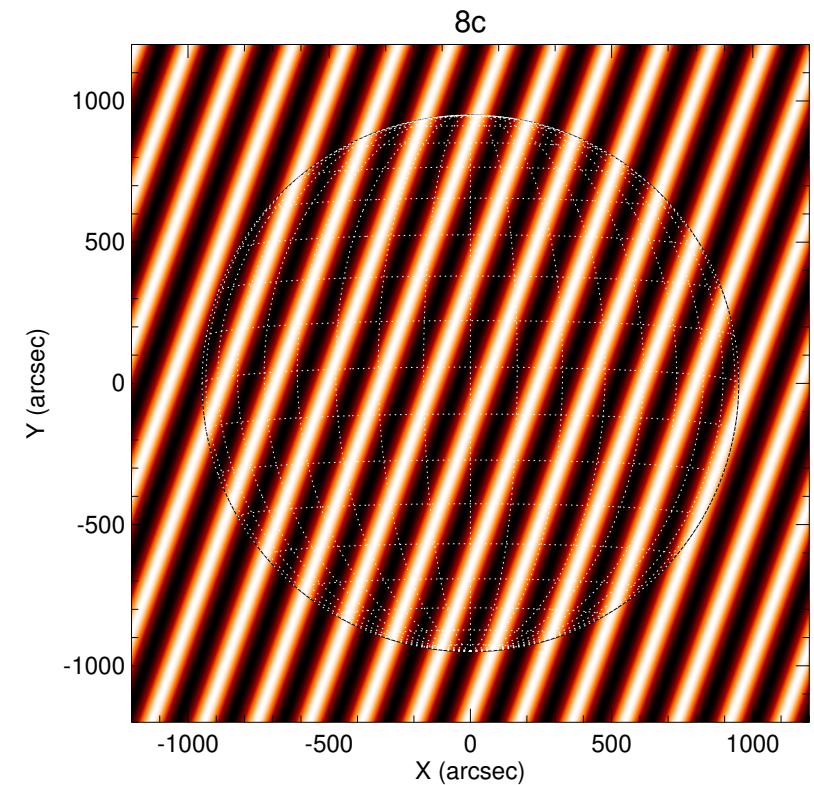
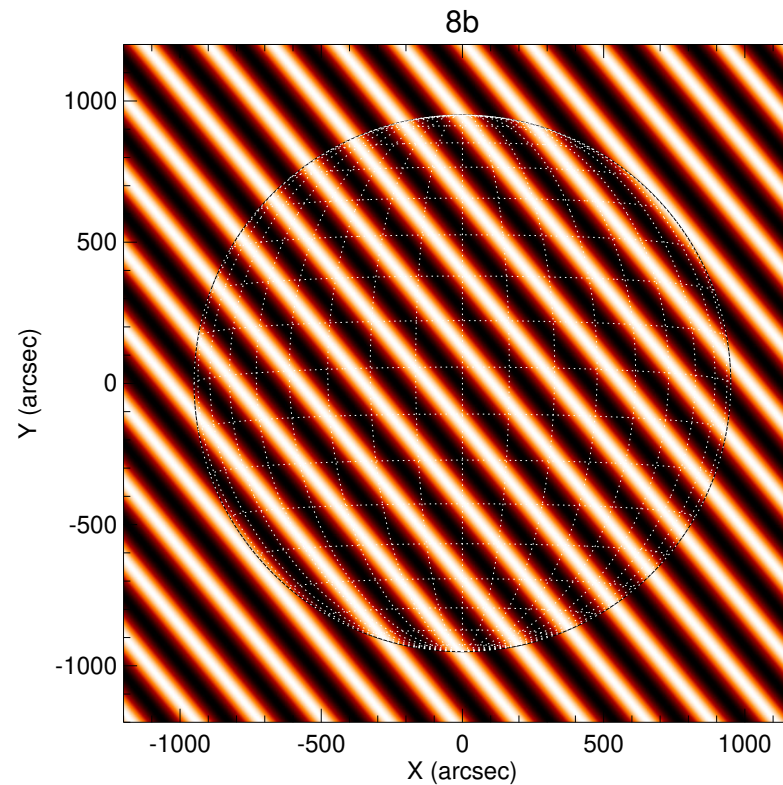
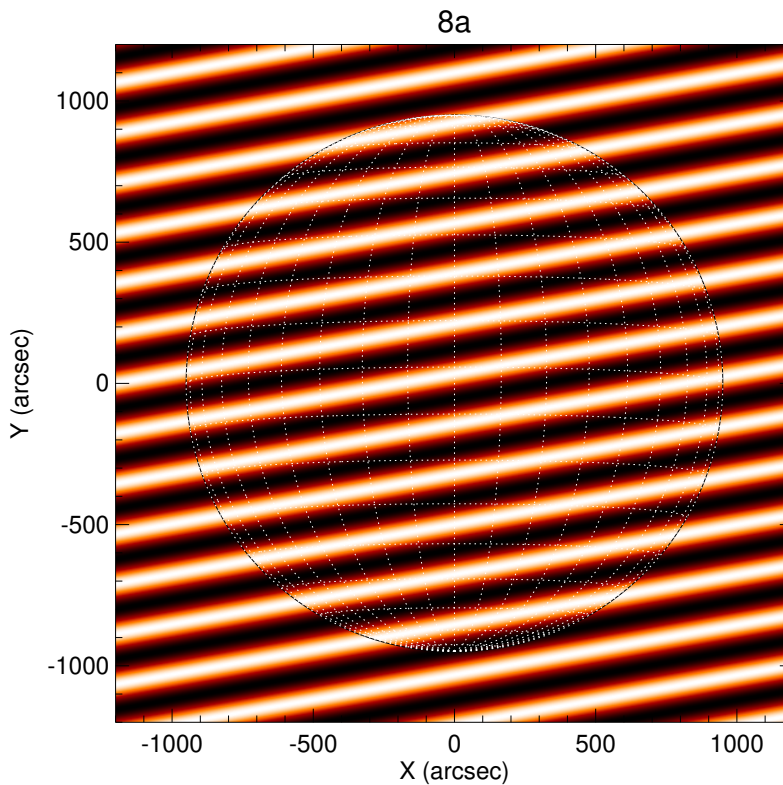
Back projection (Mertz et al., 1986)

Detectors with the same resolution produce waves with same period but different orientation



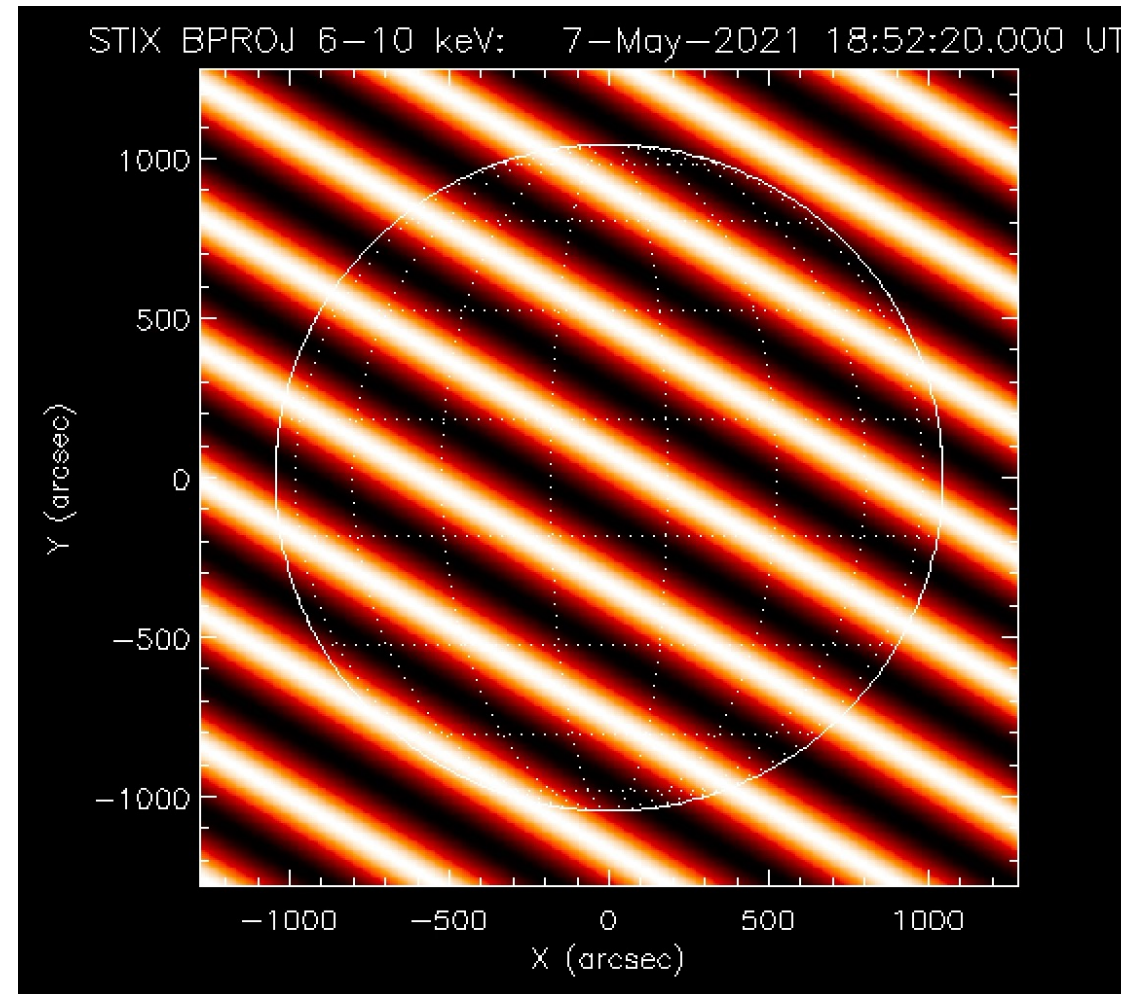
Back projection (Mertz et al., 1986)

Detectors with the same resolution produce waves with same period but different orientation



Back projection (Mertz et al., 1986)

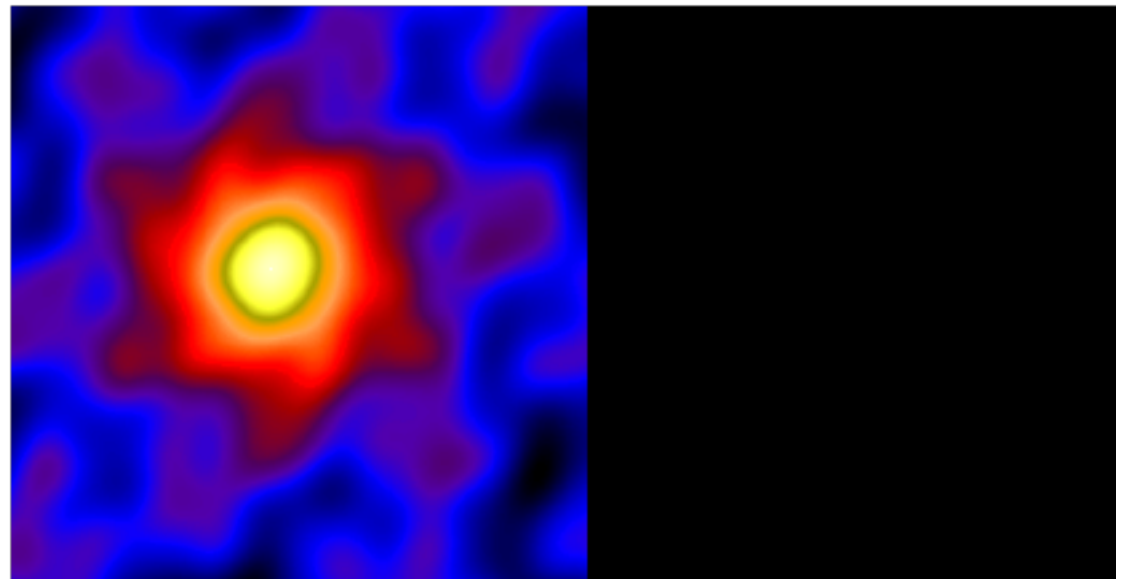
The Back Projection map is obtained by summing the waves corresponding to all the detectors



Clean (Högbom, 1974)

Iterative method:

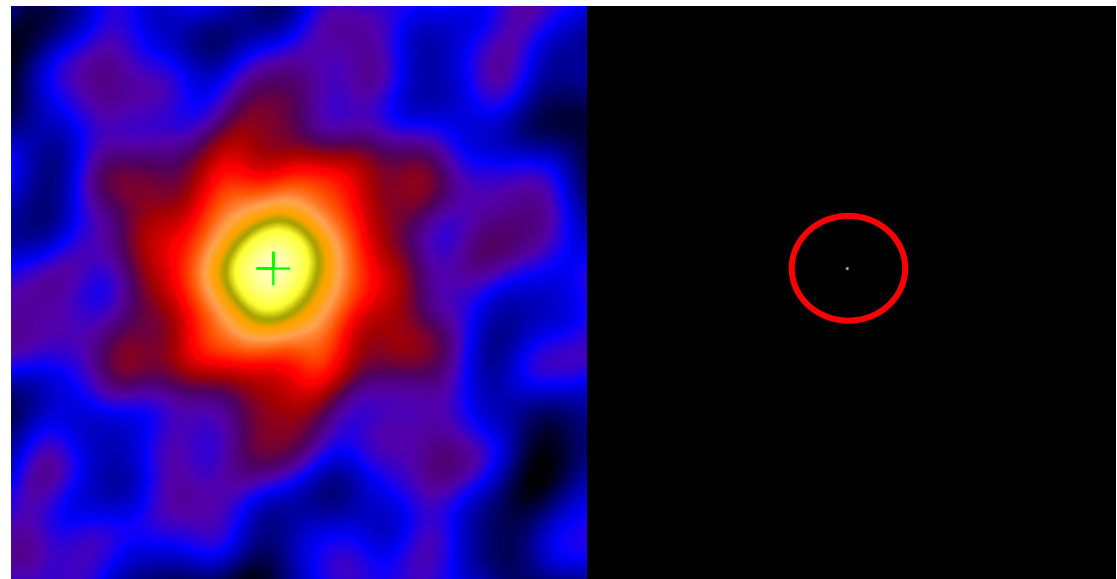
- Creates two maps: **dirty map** (back projection) and **clean components (cc) map** (zero map)



Clean (Högbom, 1974)

Iterative method:

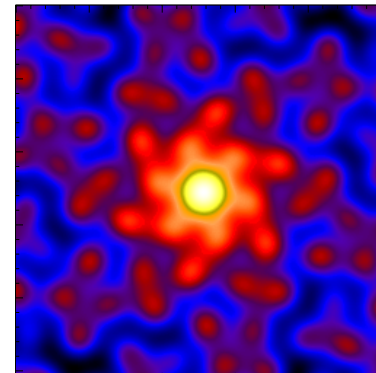
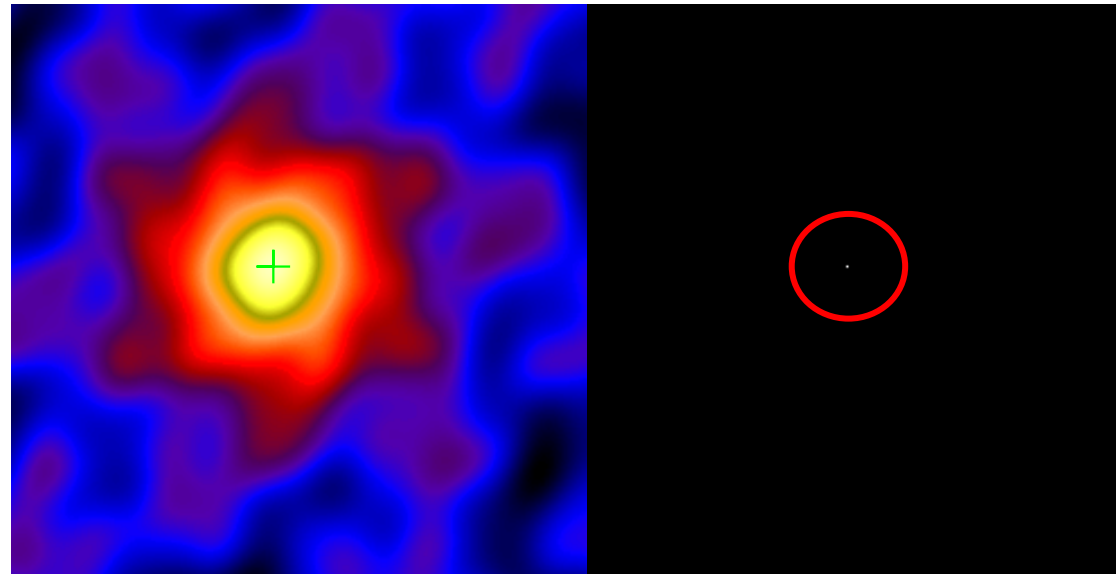
- Creates two maps: **dirty map** (back projection) and **clean components (cc) map** (zero map)
- Finds maximum of the dirty map and add clean component in the cc map



Clean (Högbom, 1974)

Iterative method:

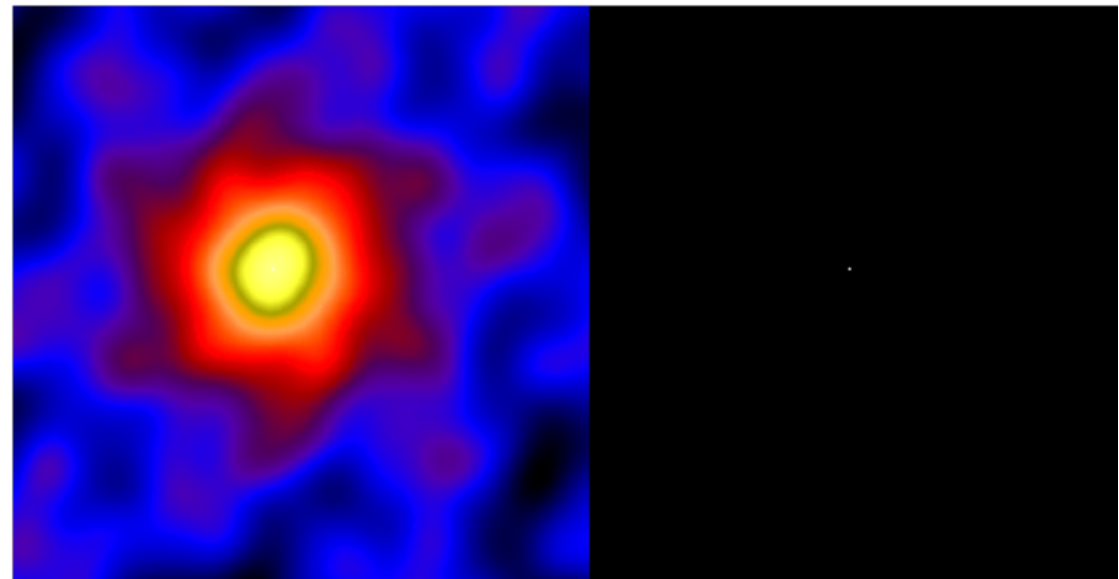
- Creates two maps: **dirty map** (back projection) and **clean components (cc) map** (zero map)
- Finds maximum of the dirty map and add clean component in the cc map
- Subtracts a fraction of the PSF from the dirty map



Clean (Högbom, 1974)

Iterative method:

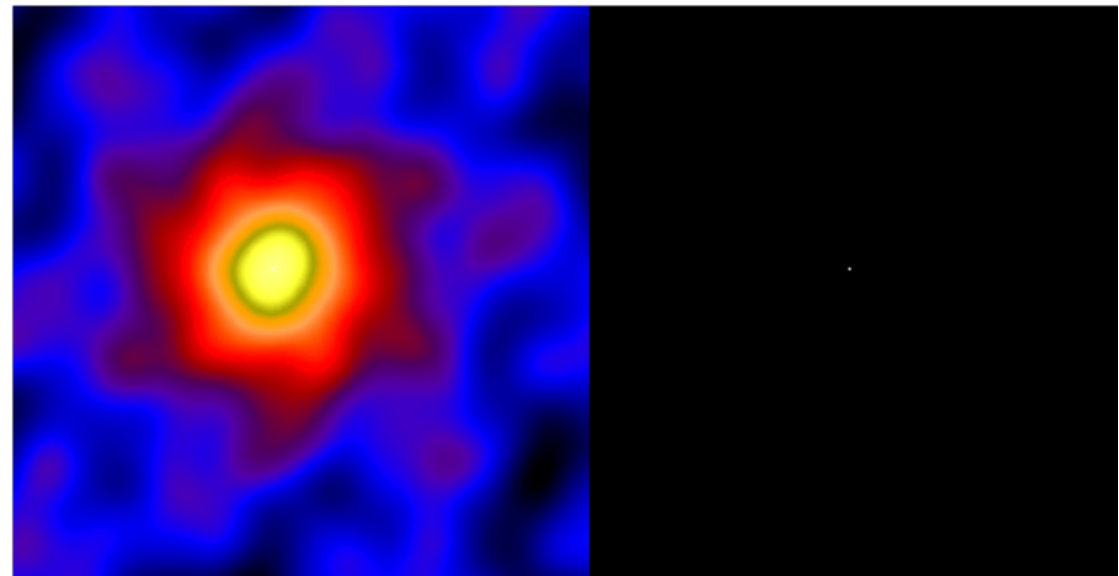
- Creates two maps: **dirty map** (back projection) and **clean components (cc) map** (zero map)
- Finds maximum of the dirty map and add clean component in the cc map
- Subtracts a fraction of the PSF from the dirty map



Clean (Högbom, 1974)

Iterative method:

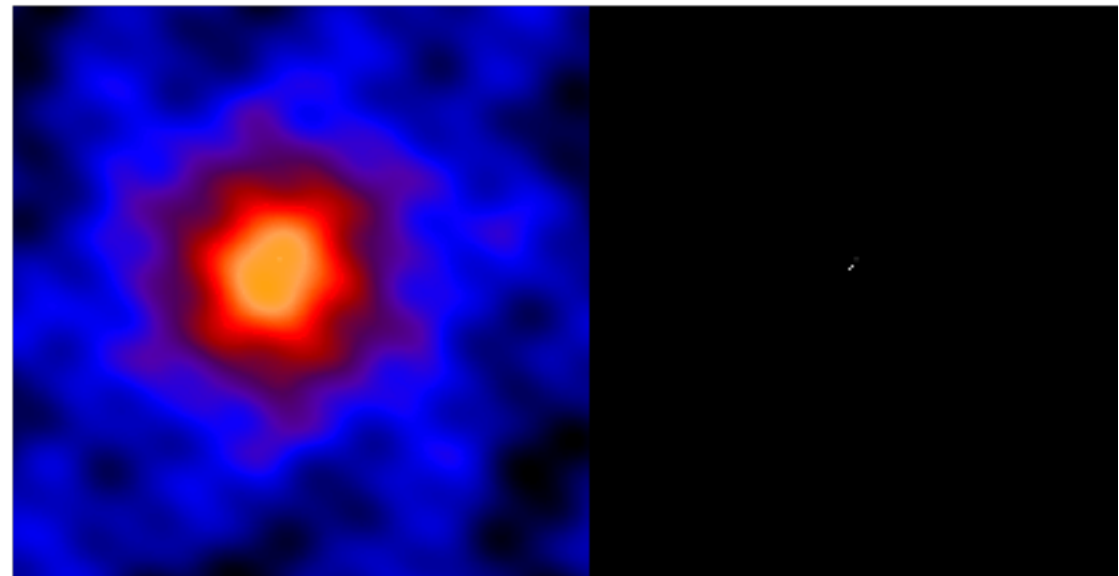
- Creates two maps: **dirty map** (back projection) and **clean components (cc) map** (zero map)
- Finds maximum of the dirty map and add clean component in the cc map
- Subtracts a fraction of the PSF from the dirty map
- Iterates



Clean (Högbom, 1974)

Iterative method:

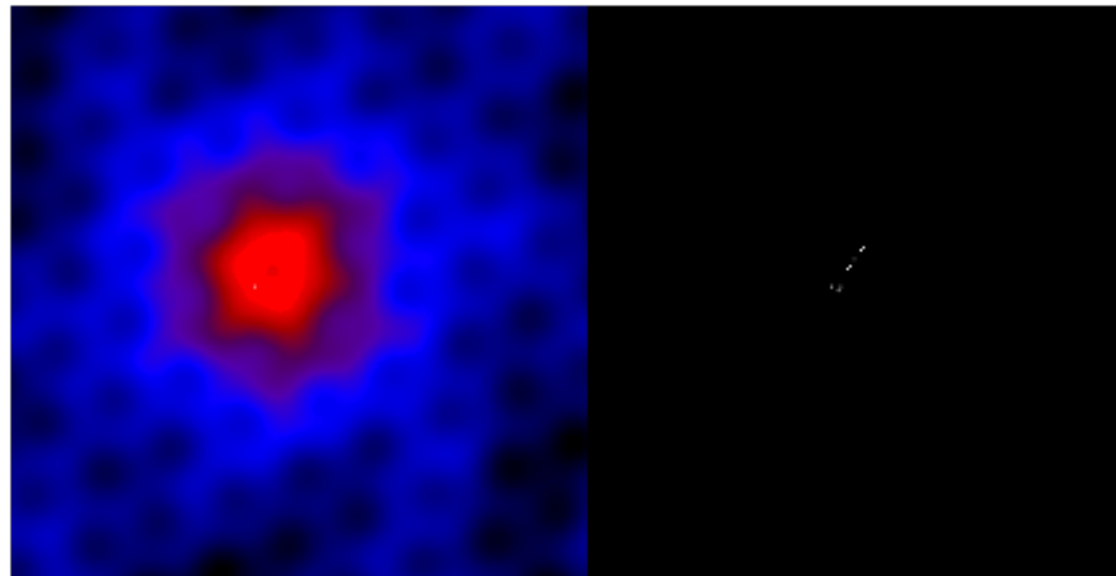
- Creates two maps: **dirty map** (back projection) and **clean components (cc) map** (zero map)
- Finds maximum of the dirty map and add clean component in the cc map
- Subtracts a fraction of the PSF from the dirty map
- Iterates



Clean (Högbom, 1974)

Iterative method:

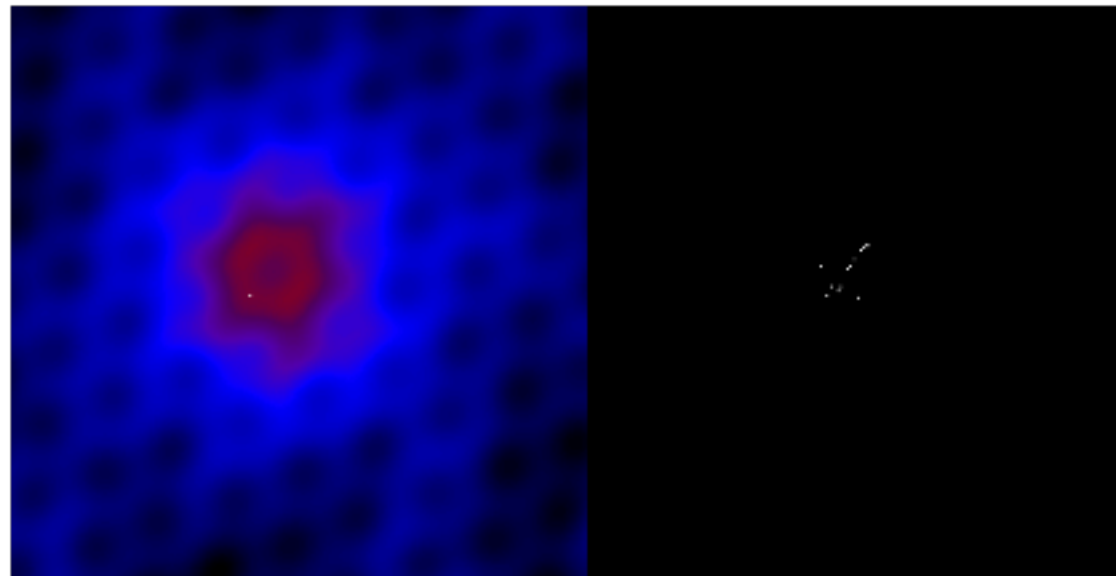
- Creates two maps: **dirty map** (back projection) and **clean components (cc) map** (zero map)
- Finds maximum of the dirty map and add clean component in the cc map
- Subtracts a fraction of the PSF from the dirty map
- Iterates



Clean (Högbom, 1974)

Iterative method:

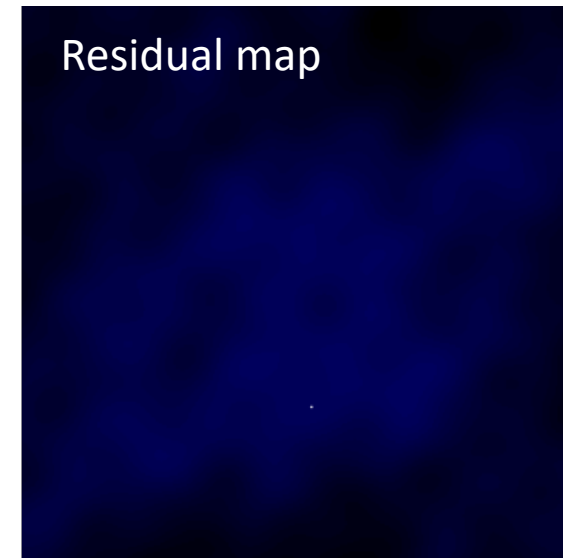
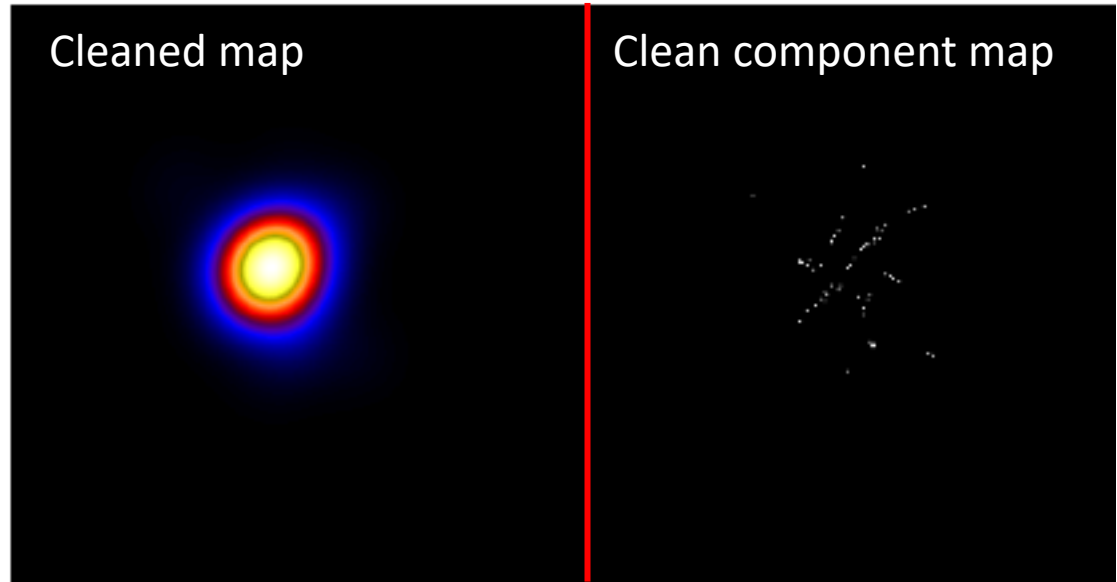
- Creates two maps: **dirty map** (back projection) and **clean components (cc) map** (zero map)
- Finds maximum of the dirty map and add clean component in the cc map
- Subtracts a fraction of the PSF from the dirty map
- Iterates



Clean (Högbom, 1974)

Iterative method:

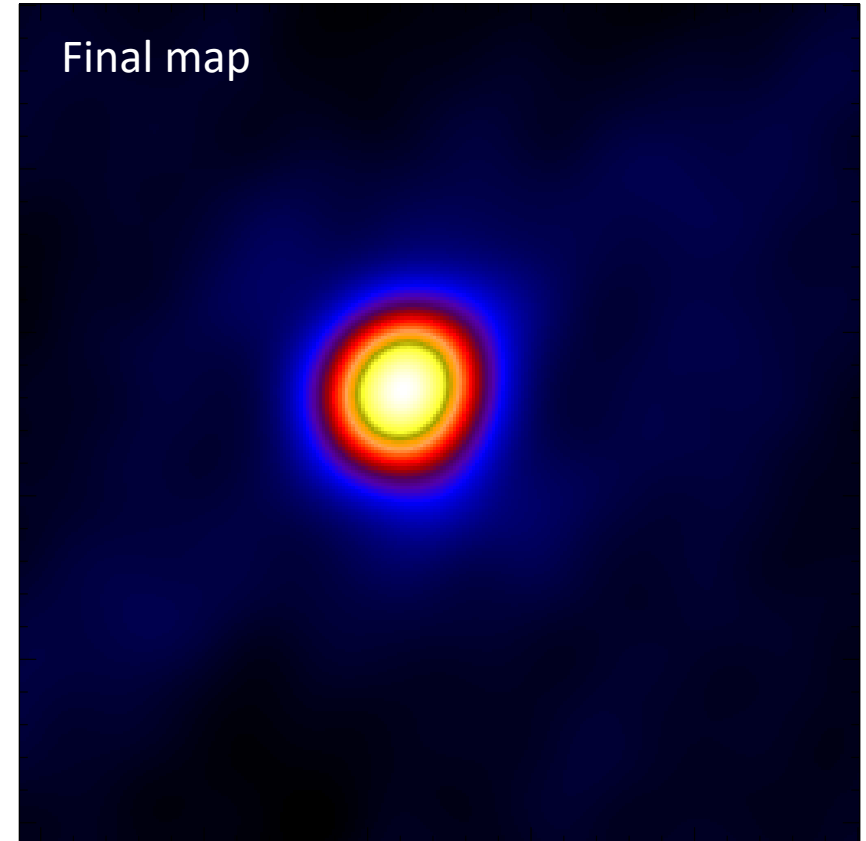
- Creates two maps: **dirty map** (back projection) and **clean components (cc) map** (zero map)
- Finds maximum of the dirty map and add clean component in the cc map
- Subtracts a fraction of the PSF from the dirty map
- Iterates
- Final step: convolution with clean beam and residuals



Clean (Högbom, 1974)

Iterative method:

- Creates two maps: **dirty map** (back projection) and **clean components (cc) map** (zero map)
- Finds maximum of the dirty map and add clean component in the cc map
- Subtracts a fraction of the PSF from the dirty map
- Iterates
- Final step: convolution with clean beam and residuals



MEMGE (Massa et al., 2020)

Solves the maximum-entropy regularized problem

$$\arg \min_{\phi \geq 0} \chi^2(\phi) - \lambda H(\phi)$$

$$\text{with } \sum_j \phi_j = f$$

where

$$\chi^2(\phi) = \sum_i \frac{|(\mathcal{F}\phi)_i - V_i|^2}{\sigma_i^2} \quad H(\phi) = - \sum_j \phi_j \log \left(\frac{\phi_j}{me} \right)$$

MEM_GE (Massa et al., 2020)

Solves the maximum-entropy regularized problem

$$\arg \min_{\phi \geq 0} \chi^2(\phi) - \lambda H(\phi)$$

with $\sum_j \phi_j = f$

where

$$\chi^2(\phi) = \sum_i \frac{|(\mathcal{F}\phi)_i - V_i|^2}{\sigma_i^2}$$

$$H(\phi) = - \sum_j \phi_j \log \left(\frac{\phi_j}{me} \right)$$

Data fitting

MEM_GE (Massa et al., 2020)

Solves the maximum-entropy regularized problem

$$\arg \min_{\phi \geq 0} \chi^2(\phi) - \lambda H(\phi)$$

$$\text{with } \sum_j \phi_j = f$$

where

$$\chi^2(\phi) = \sum_i \frac{|(\mathcal{F}\phi)_i - V_i|^2}{\sigma_i^2}$$

$$H(\phi) = - \sum_j \phi_j \log \left(\frac{\phi_j}{me} \right)$$

Regularization

MEMGE (Massa et al., 2020)

Solves the maximum-entropy regularized problem

$$\arg \min_{\phi \geq 0} \chi^2(\phi) - \lambda H(\phi)$$

with $\sum_j \phi_j = f$

Regularization parameter

where

$$\chi^2(\phi) = \sum_i \frac{|(\mathcal{F}\phi)_i - V_i|^2}{\sigma_i^2} \quad H(\phi) = - \sum_j \phi_j \log \left(\frac{\phi_j}{me} \right)$$

MEM_GE (Massa et al., 2020)

Solves the maximum-entropy regularized problem

Positivity constraint $\longrightarrow \boxed{\phi \geq 0}$

$$\arg \min \chi^2(\phi) - \lambda H(\phi)$$
$$\text{with } \sum_j \phi_j = f$$

where

$$\chi^2(\phi) = \sum_i \frac{|(\mathcal{F}\phi)_i - V_i|^2}{\sigma_i^2} \quad H(\phi) = - \sum_j \phi_j \log \left(\frac{\phi_j}{me} \right)$$

MEM_GE (Massa et al., 2020)

Solves the maximum-entropy regularized problem

$$\arg \min_{\phi \geq 0} \chi^2(\phi) - \lambda H(\phi)$$

$$\text{with } \sum_j \phi_j = f$$

← Flux constraint

where

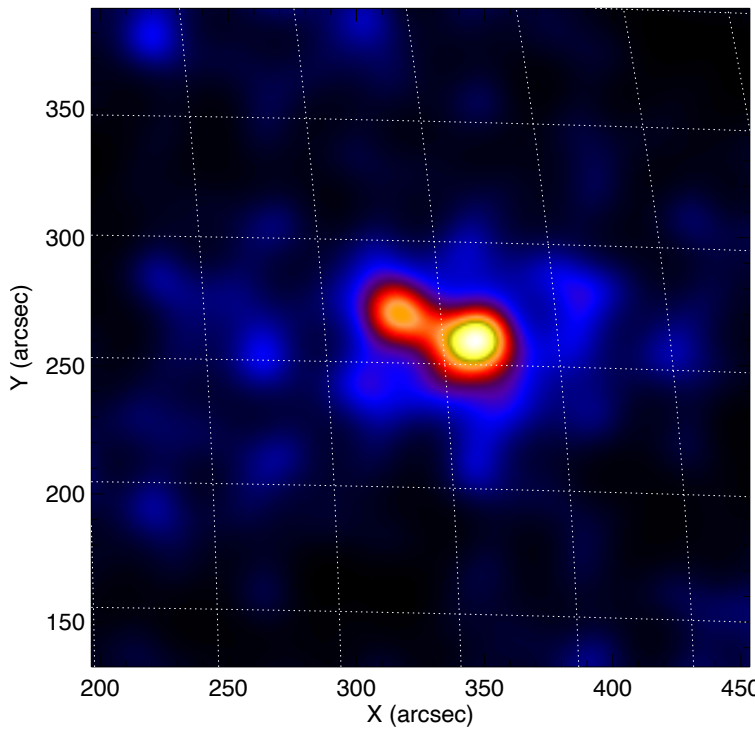
$$\chi^2(\phi) = \sum_i \frac{|(\mathcal{F}\phi)_i - V_i|^2}{\sigma_i^2}$$

$$H(\phi) = - \sum_j \phi_j \log \left(\frac{\phi_j}{m e} \right)$$

MEM_GE (Massa et al., 2020)

λ : finds a tradeoff between data fitting and regularization

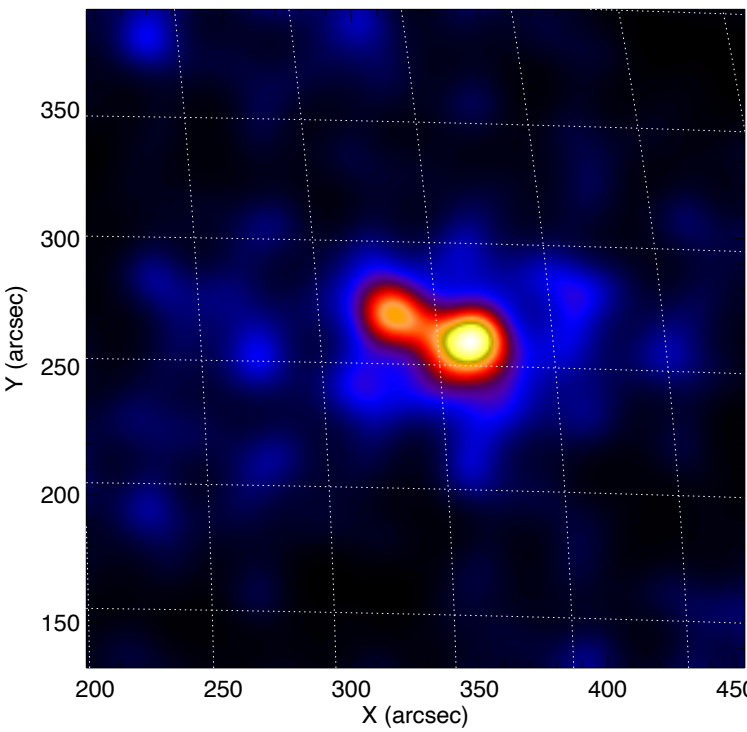
Large λ



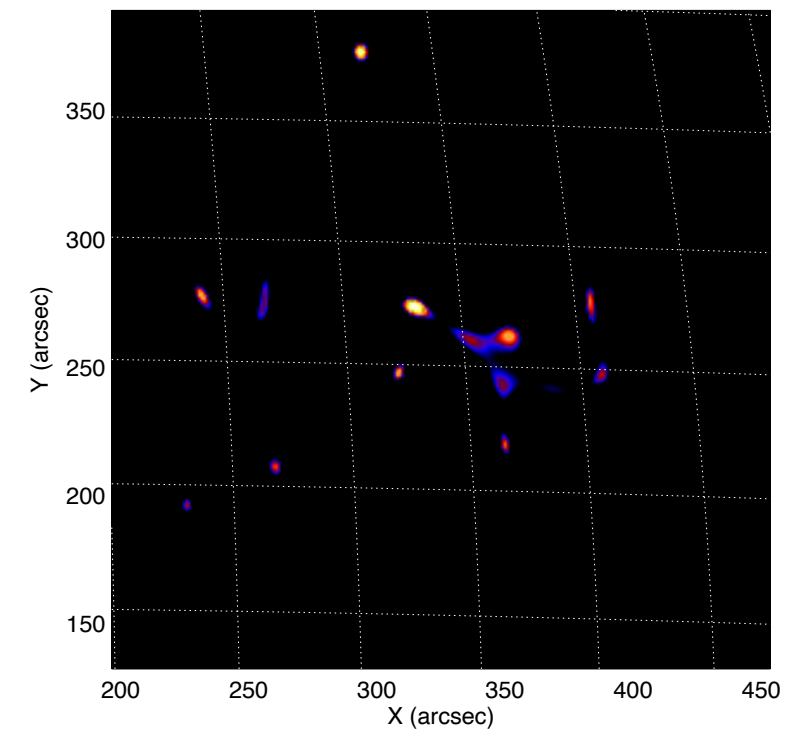
MEM_GE (Massa et al., 2020)

λ : finds a tradeoff between data fitting and regularization

Large λ

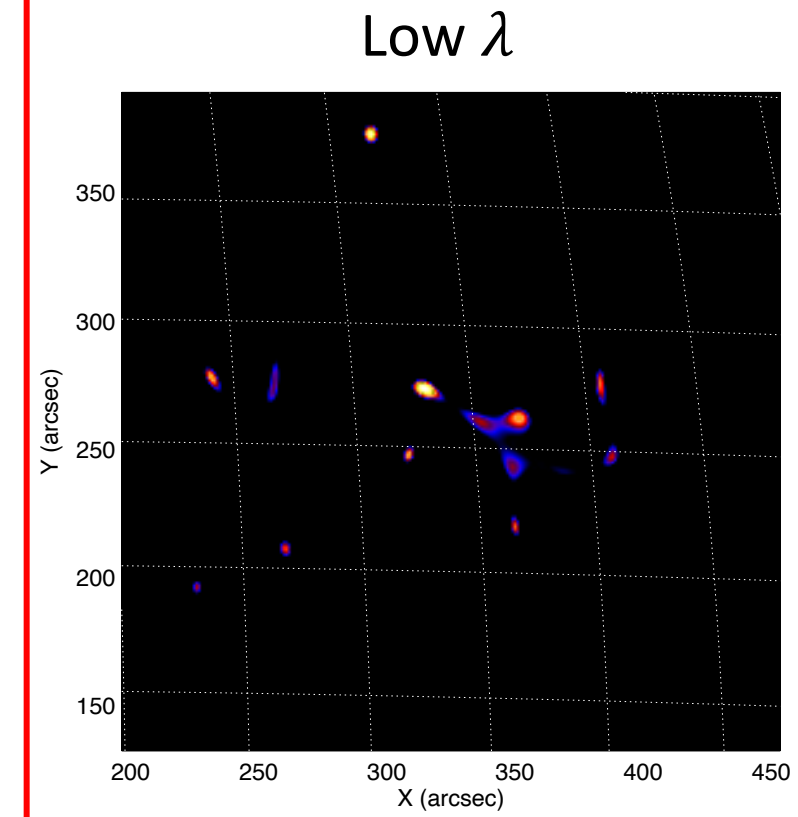
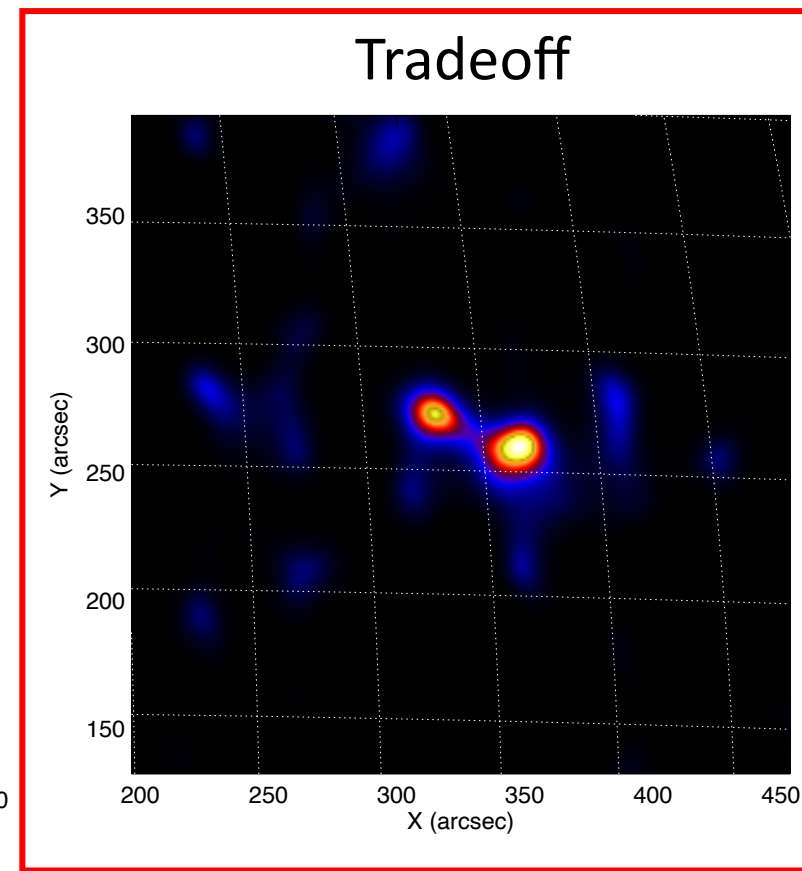
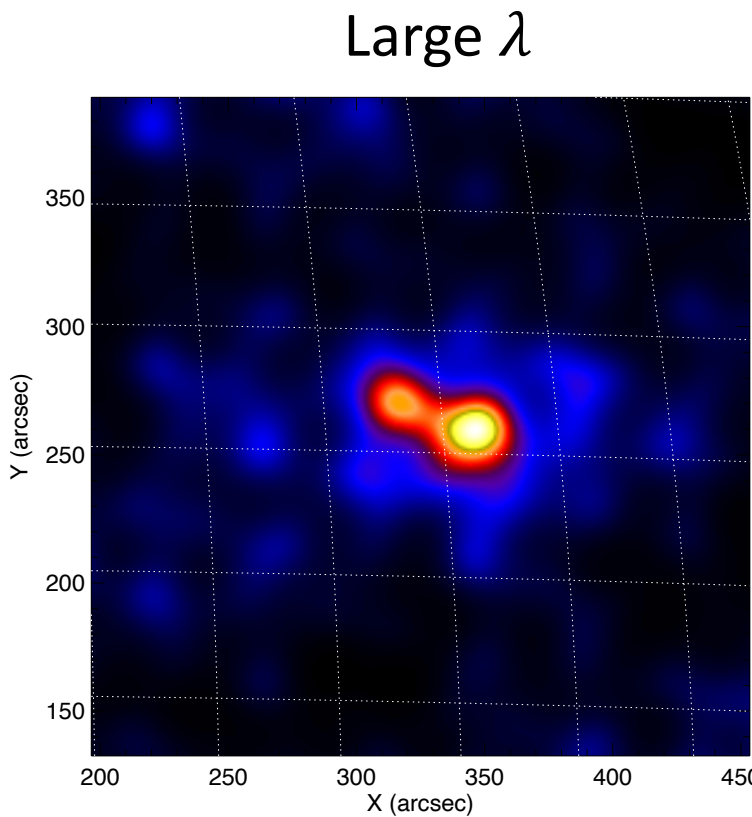


Low λ



MEM_GE (Massa et al., 2020)

λ : finds a tradeoff between data fitting and regularization



Expectation Maximization (Massa et al., 2019)

- Count-based iterative method which solves

$$M\phi = \mathbf{C}$$

Expectation Maximization (Massa et al., 2019)

- Count-based iterative method which solves

$$M\phi = C$$


Matrix modelling the grid transmission

Expectation Maximization (Massa et al., 2019)

- Count-based iterative method which solves

$$M\phi = \mathbf{C}$$

Array containing the measured counts

Expectation Maximization (Massa et al., 2019)

- Count-based iterative method which solves

$$M\phi = \mathbf{C}$$

- Maximum likelihood approach:

$$P(\mathbf{C}|\phi) = \prod_l \exp(-M\phi_l) \frac{(M\phi_l)^{C_l}}{C_l!} \longrightarrow \text{Solve: } \arg \max_{\phi \geq 0} P(\mathbf{C}|\phi)$$

Expectation Maximization (Massa et al., 2019)

- Count-based iterative method which solves

$$M\phi = \mathbf{C}$$

- Maximum likelihood approach:

$$P(\mathbf{C}|\phi) = \prod_l \exp(-M\phi_l) \frac{(M\phi_l)^{C_l}}{C_l!} \longrightarrow \text{Solve: } \arg \max_{\phi \geq 0} P(\mathbf{C}|\phi)$$

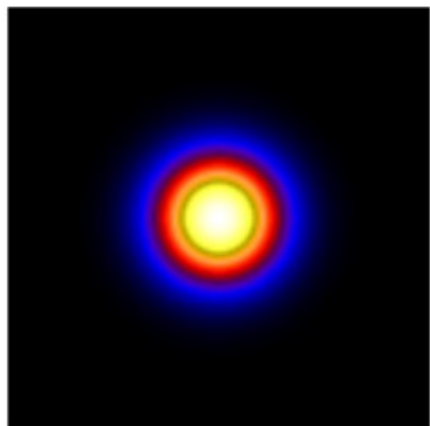
- EM is the same algorithm as Richardson-Lucy:

$$\phi_{k+1} = \frac{\phi_k}{M^T \mathbf{1}} M^T \left(\frac{\mathbf{C}}{M\phi_k} \right)$$

Forward Fit (Hurford et al., 2002)

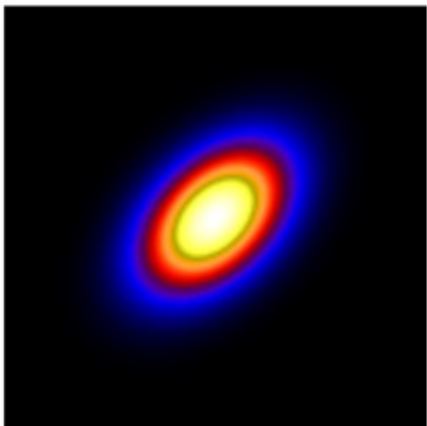
- Parametric source shapes

Circular Gaussian



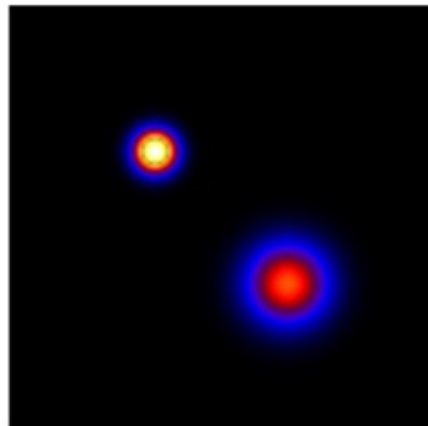
$$\theta = (x^c, y^c, f, \sigma)$$

Elliptical Gaussian



$$\theta = (x^c, y^c, f, \sigma, \varepsilon, \alpha)$$

Double circular Gaussian

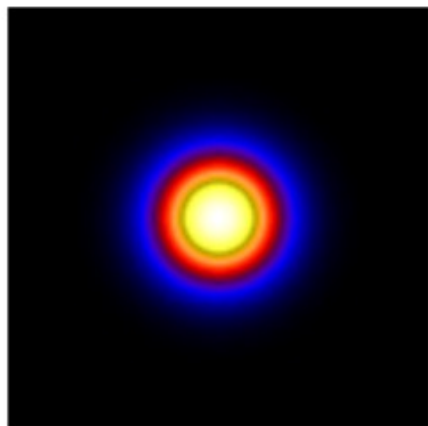


$$\theta = (x_1^c, y_1^c, f_1, \sigma_1, x_2^c, y_2^c, f_2, \sigma_2)$$

Forward Fit (Hurford et al., 2002)

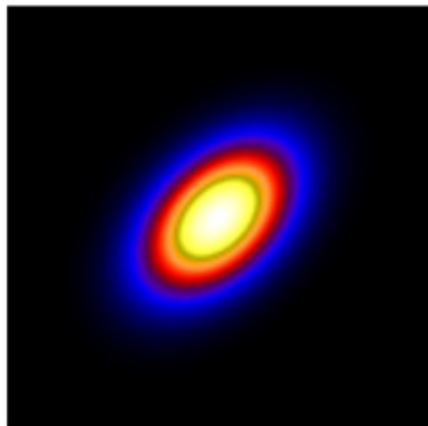
- Parametric source shapes

Circular Gaussian



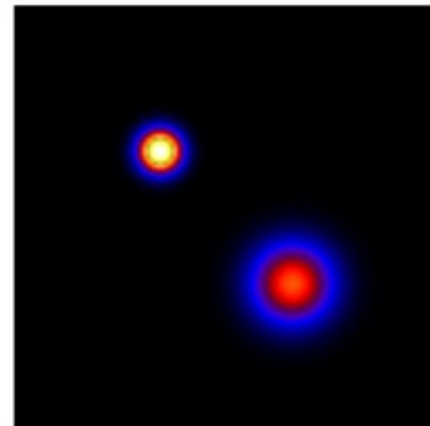
$$\theta = (x^c, y^c, f, \sigma)$$

Elliptical Gaussian



$$\theta = (x^c, y^c, f, \sigma, \varepsilon, \alpha)$$

Double circular Gaussian



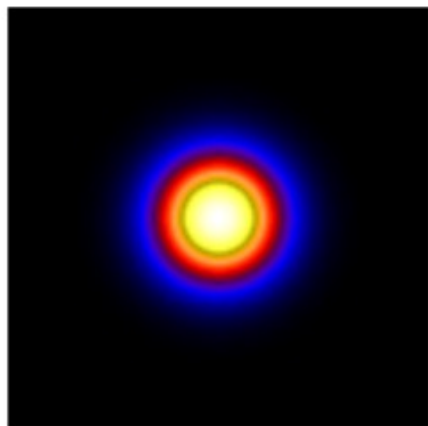
$$\theta = (x_1^c, y_1^c, f_1, \sigma_1, x_2^c, y_2^c, f_2, \sigma_2)$$

- Solves: $\arg \min_{\theta} \chi^2(\theta) := \sum_i \frac{|(\mathcal{F}\phi(\theta))_i - V_i|^2}{\sigma_i^2}$

Forward Fit (Hurford et al., 2002)

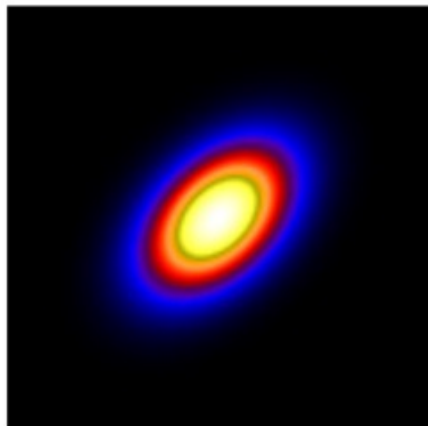
- Parametric source shapes

Circular Gaussian



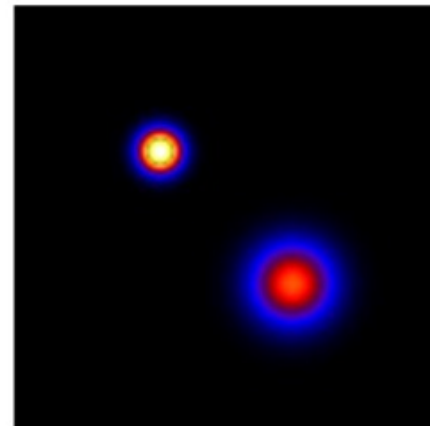
$$\theta = (x^c, y^c, f, \sigma)$$

Elliptical Gaussian



$$\theta = (x^c, y^c, f, \sigma, \varepsilon, \alpha)$$

Double circular Gaussian



$$\theta = (x_1^c, y_1^c, f_1, \sigma_1, x_2^c, y_2^c, f_2, \sigma_2)$$

- Solves: $\arg \min_{\theta} \chi^2(\theta) := \sum_i \frac{|(\mathcal{F}\phi(\theta))_i - V_i|^2}{\sigma_i^2}$

Source shape parameterized by θ

Forward Fit (Hurford et al., 2002)

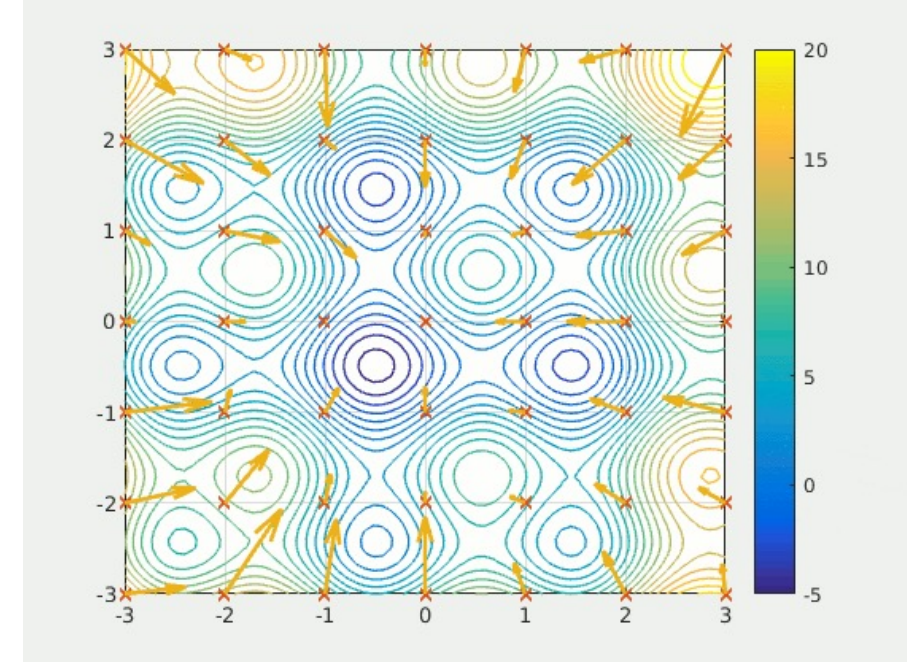
- **Uncertainty on the parameters:** 20 reconstructions from visibilities perturbed with Gaussian noise and computation of the standard deviation

Forward Fit (Hurford et al., 2002)

- **Uncertainty on the parameters:** 20 reconstructions from visibilities perturbed with Gaussian noise and computation of the standard deviation
- Implementation inherited from RHESSI: relies on the AMOEBA_C routine for the optimization of the parameters (simplex method, sometimes provides suboptimal results)

Forward Fit (Hurford et al., 2002)

- **Uncertainty on the parameters:** 20 reconstructions from visibilities perturbed with Gaussian noise and computation of the standard deviation
- Implementation inherited from RHESSI: relies on the AMOEBA_C routine for the optimization of the parameters (simplex method, sometimes provides suboptimal results)
- **New optimization method (under development):** based on Particle Swarm Optimization (PSO, Eberhart et al., 1995)

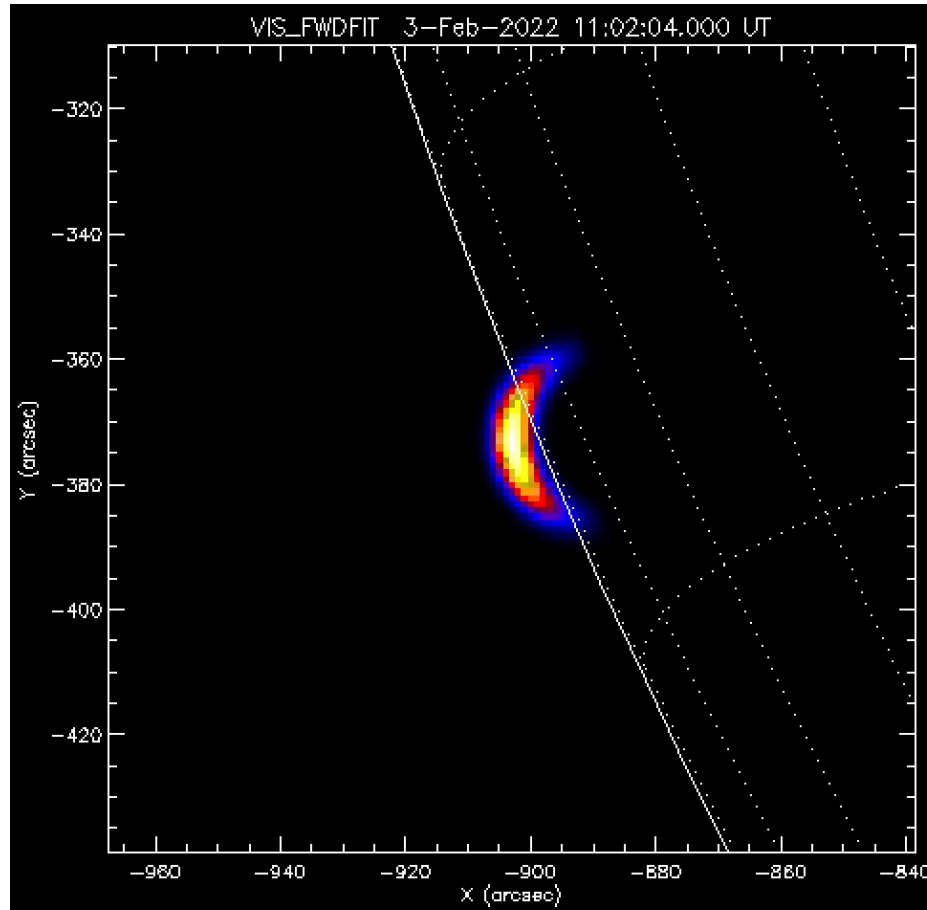


By Ephramac - Own work, CC BY-SA 4.0,
<https://commons.wikimedia.org/w/index.php?curid=54975083>

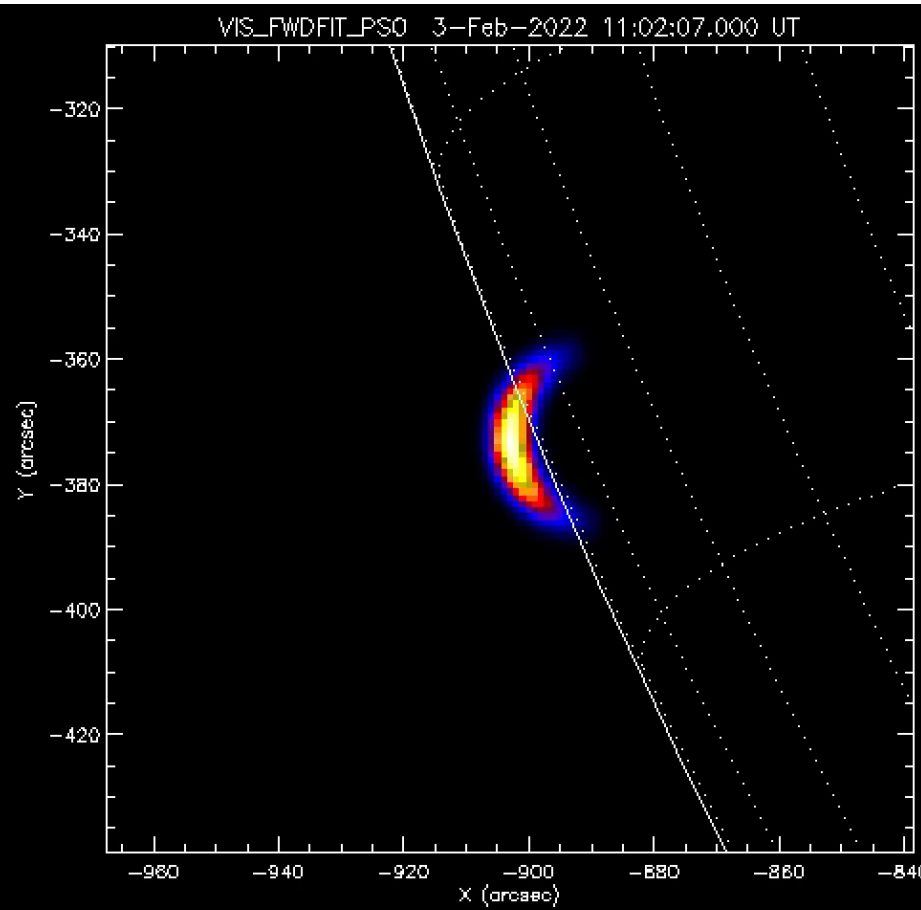
Forward Fit – PSO vs AMOEBA

Test: map center shift

AMOEBA_C optimizer



PSO optimizer

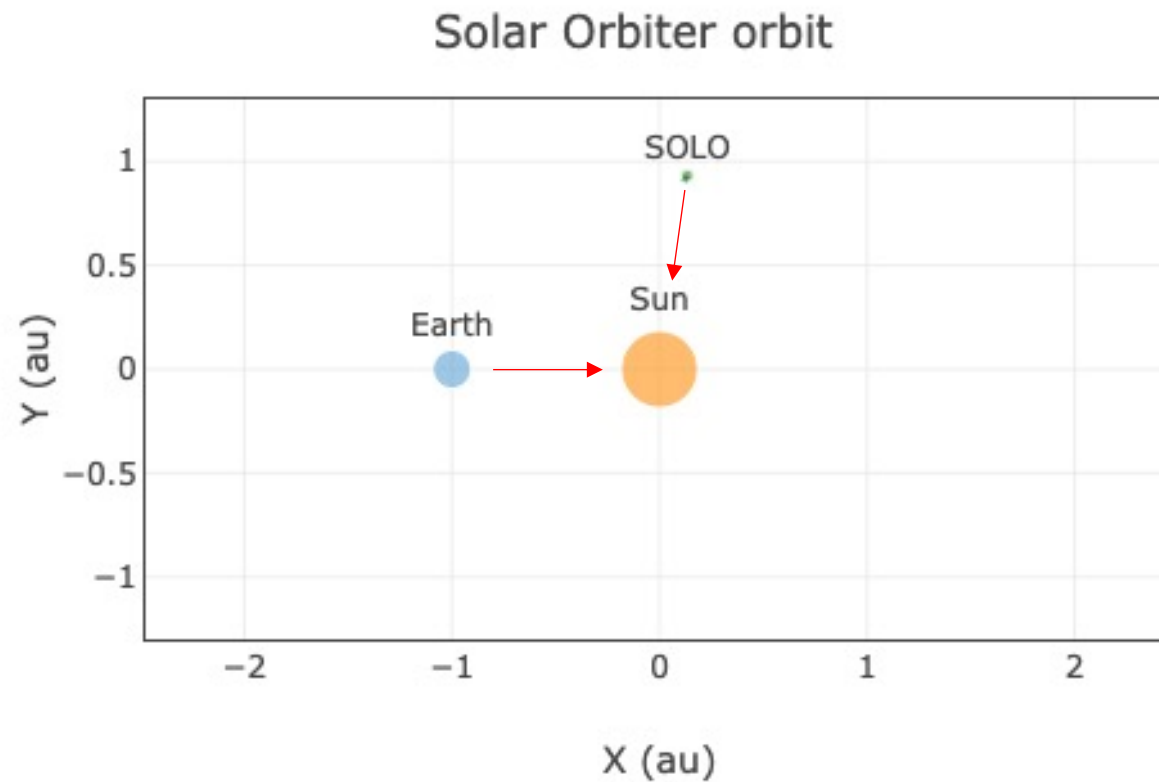


Amplitude Forward Fit (Massa et al, 2021)

- Forward fitting method from visibility amplitudes (used before the phase calibration had been completed)
- Same shapes as in the standard Forward Fit
- Visibility amplitudes do not contain any information on the absolute location of the source → shapes centered in the origin of the coordinate system
- Optimization based on PSO

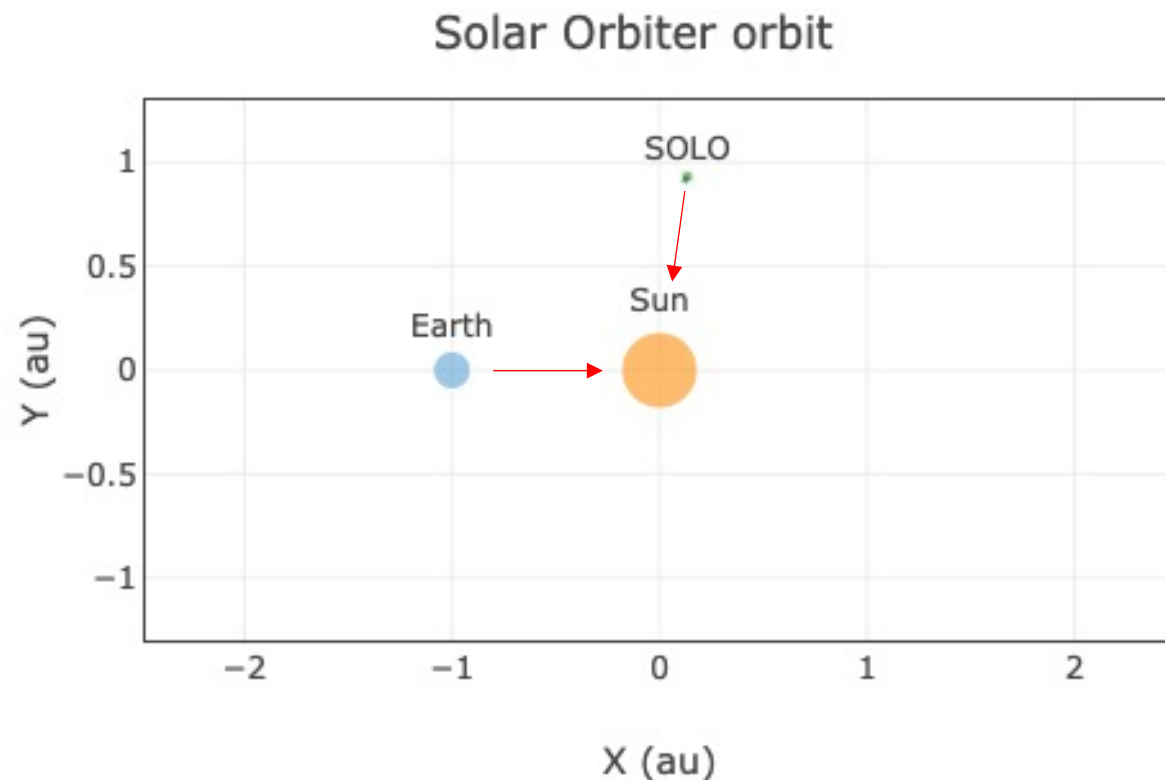
May 2021 events (Massa et al., in preparation)

Angle relative to Earth-Sun (in May 2021): $97.4^\circ - 98.2^\circ$



May 2021 events (Massa et al., in preparation)

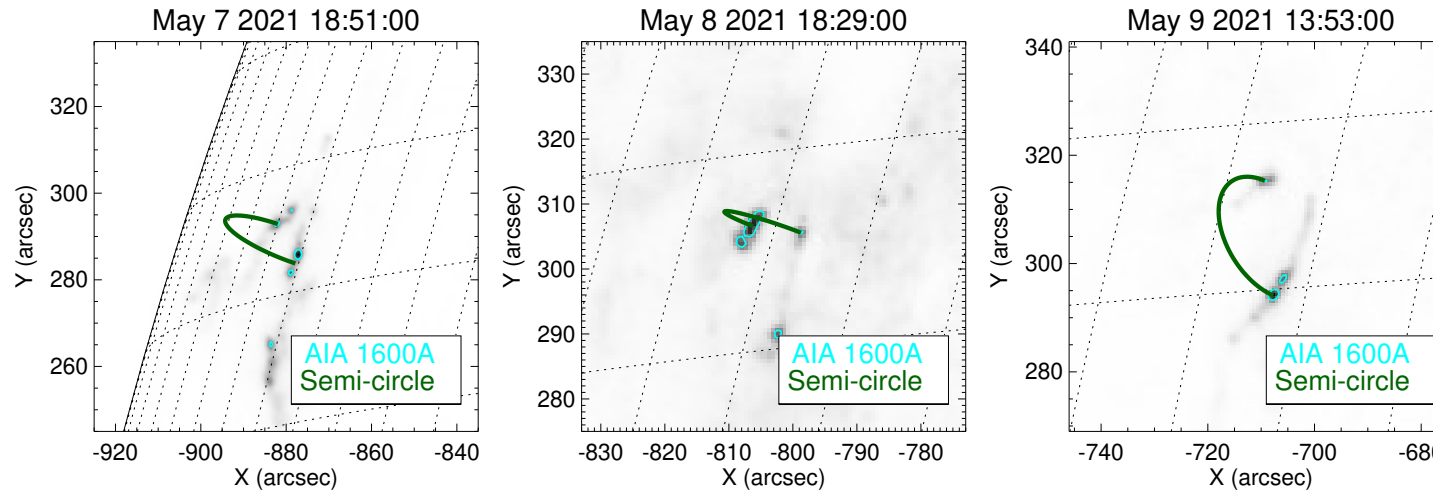
Angle relative to Earth-Sun (in May 2021): $97.4^\circ - 98.2^\circ$



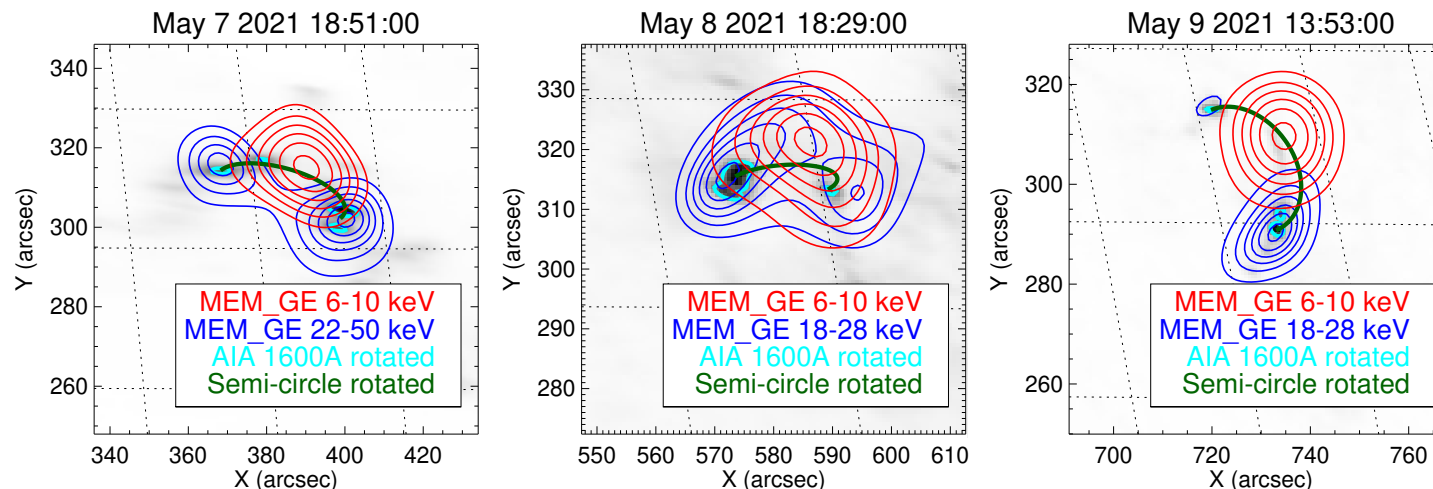
AIA images rotated by means of the
reproject Python package (see
Battaglia et al., 2021)

May 2021 events (Massa et al., in preparation)

Earth vantage point



Solar Orbiter vantage point



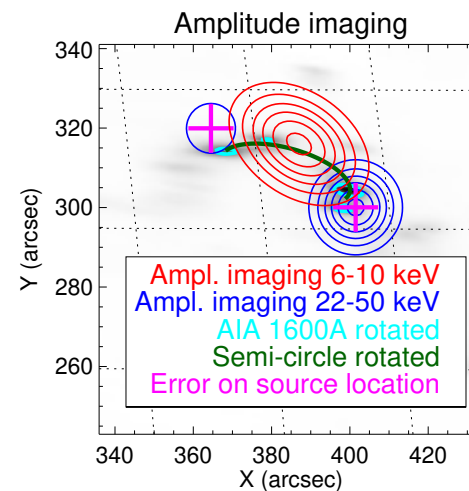
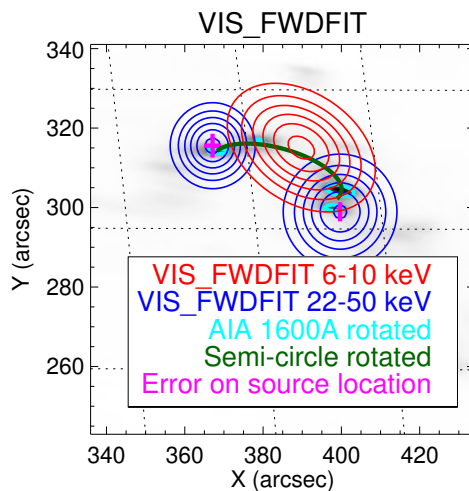
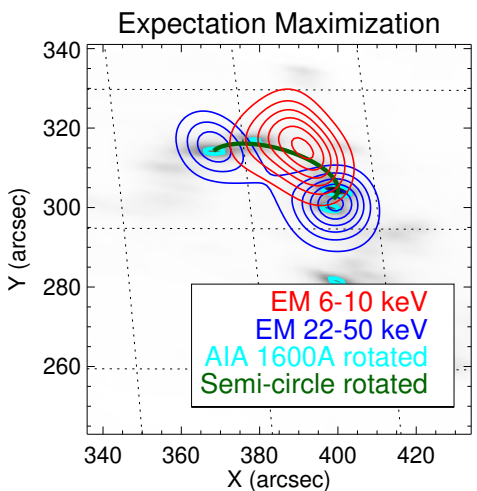
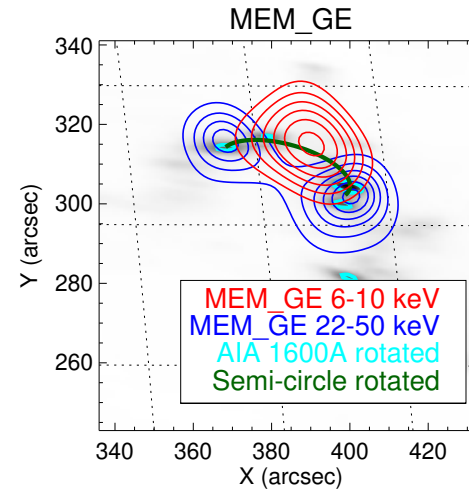
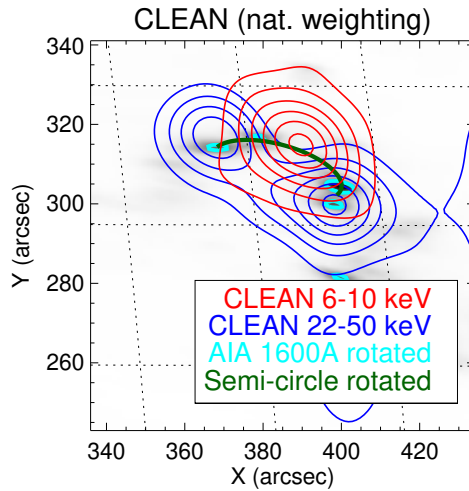
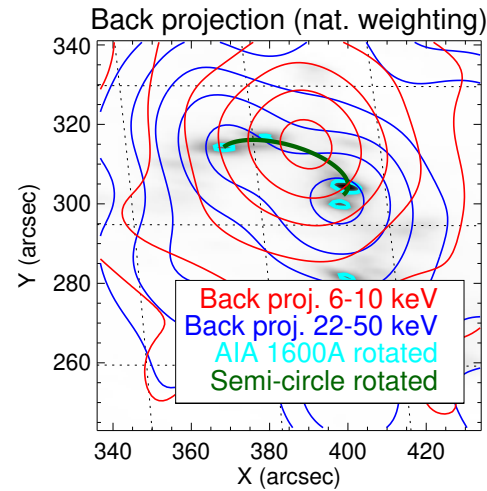
Active region AR2822

- May 7: GOES M3.9
- May 8: GOES C8.6
- May 9: GOES C4.0

Manual shift STIX reconstructions

Event	Δx (arcsec)	Δy (arcsec)
May 7	44	54
May 8	45	57
May 9	47.5	53

May 2021 events (Massa et al., in preparation)



Thermal component

Method	χ^2
Clean	3.95
MEM_GE	1.73
EM	5.08
VIS_FWDFIT	8.39

Non-thermal component

Method	χ^2
Clean	2.33
MEM_GE	1.54
EM	2.08
VIS_FWDFIT	2.84

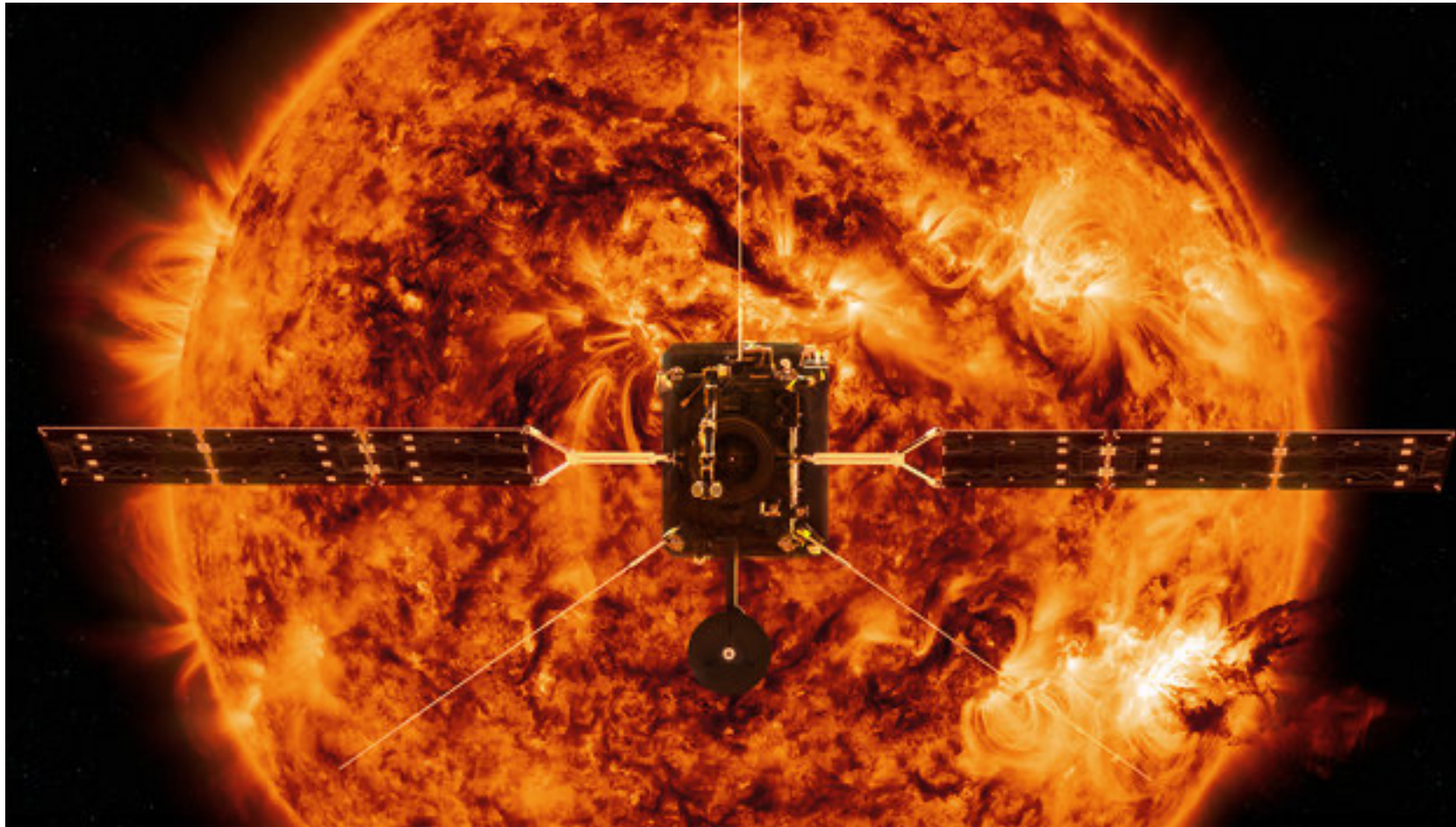
Conclusions

- We presented the STIX imaging concept and the image reconstruction problem from STIX visibilities
- We described the methods implemented for the solution of the image reconstruction problem (RHESSI legacy and some improvements)
- We showed the first results obtained with the 24 coarsest detectors on several events recorded in May 2021
- Next step:
 - Calibration of the 6 finest detectors
 - Improvement of the state-of-the-art visibility calibration
 - Automatic image placement
 - Implementation of new methods

References

- Krucker et al., *The Spectrometer/Telescope for Imaging X-rays (STIX)*, A&A, 2020
- Meuris et al., *Caliste-SO, a CdTe based spectrometer for bright solar event observations in hard X-rays*, Nucl. Instrum. Methods Phys. Res. A, 2015
- Lin et al., *The Reuven Ramaty High-Energy Solar Spectroscopic Imager (RHESSI)*, Solar Physics, 2002
- Mertz et al., *Rotational aperture synthesis for x rays*, JOSA A, 1986
- Högbom, *Aperture synthesis with a non-regular distribution of interferometer baselines*, Astronomy and Astrophysics Supplement, 1974
- Massa et al., *MEM GE: A New Maximum Entropy Method for Image Reconstruction from Solar X-Ray Visibilities*, APJ, 2020
- Massa et al., *Count-based imaging model for the Spectrometer/Telescope for Imaging X-rays (STIX) in Solar Orbiter*, A&A, 2019
- Hurford et al, *The RHESSI imaging concept*, Solar Physics, 2002
- Eberhart et al, *Particle swarm optimization*, IEEE Proceeding, 1995
- Massa et al., *Imaging from STIX visibility amplitudes*, A&A, 2021
- Massa et al., *First hard X-ray imaging results by Solar Orbiter STIX*, in preparation
- Battaglia et al., *STIX X-ray microflare observations during the Solar Orbiter commissioning phase*, A&A, 2021

Thank you for the attention!



Visibility calibration

Amplitude calibration:

- background subtraction
- grid transmission (including the flare location)
- ELUT
- livetime

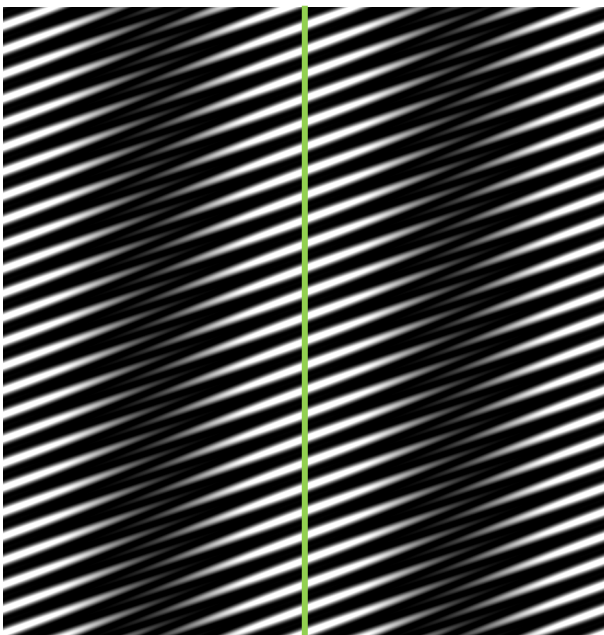
Phase calibration: keeps into account the grid geometry

Visibility calibration

Amplitude calibration:

- background subtraction
- grid transmission (including the flare location)
- ELUT
- livetime

Phase calibration: keeps into account the grid geometry

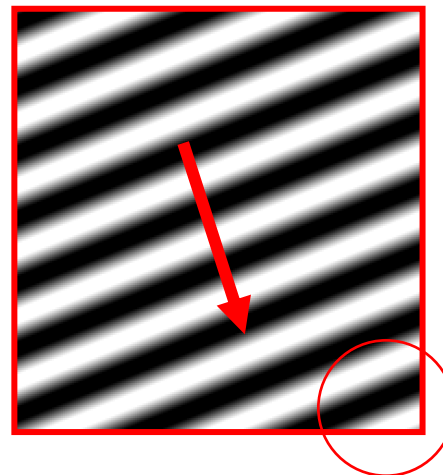
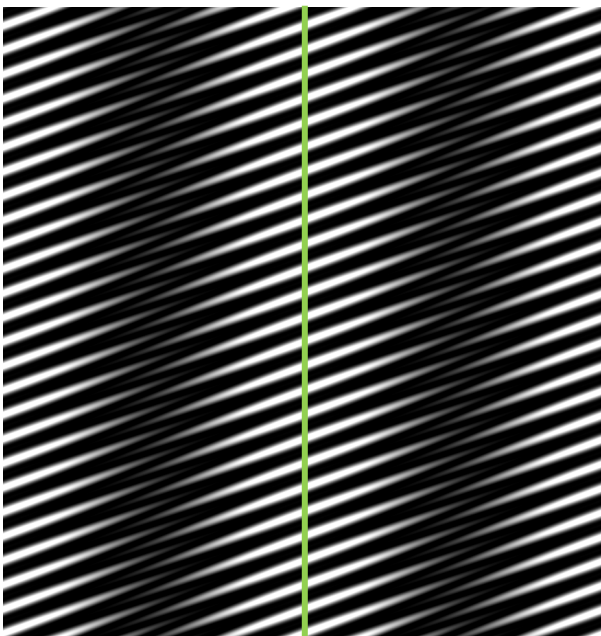


Visibility calibration

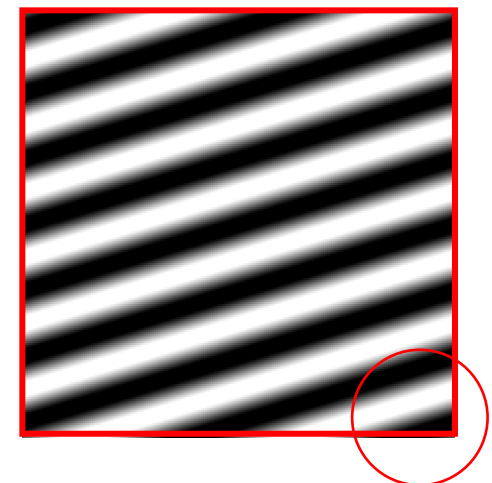
Amplitude calibration:

- background subtraction
- grid transmission (including the flare location)
- ELUT
- livetime

Phase calibration: keeps into account the grid geometry



Shift front grid

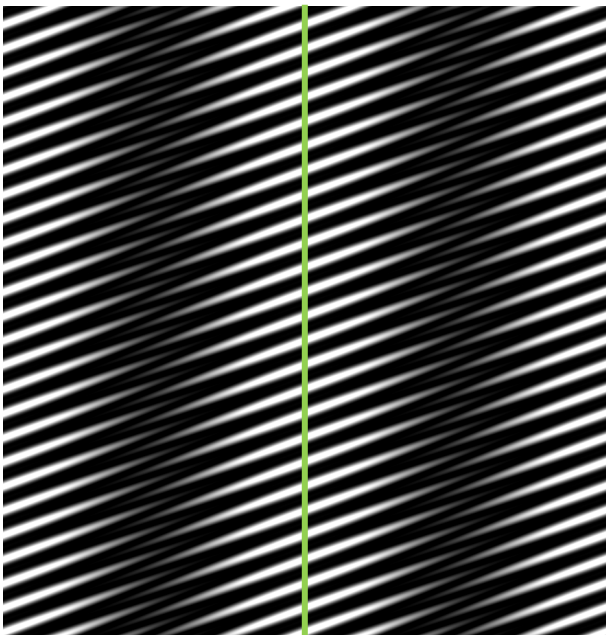


Visibility calibration

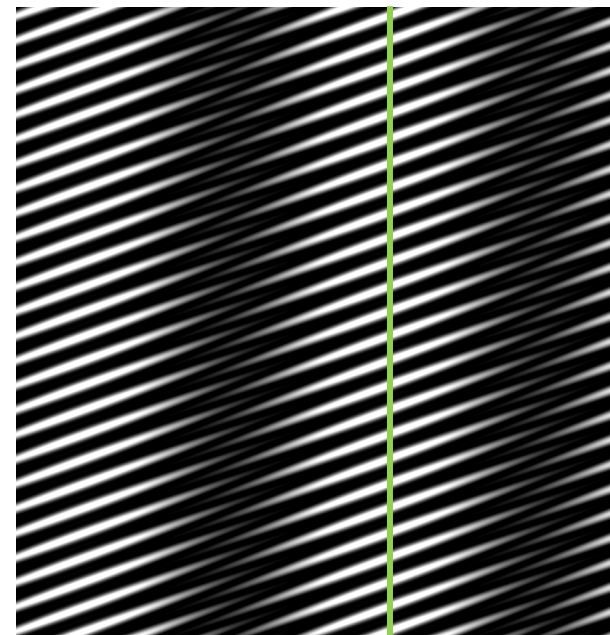
Amplitude calibration:

- background subtraction
- grid transmission (including the flare location)
- ELUT
- livetime

Phase calibration: keeps into account the grid geometry

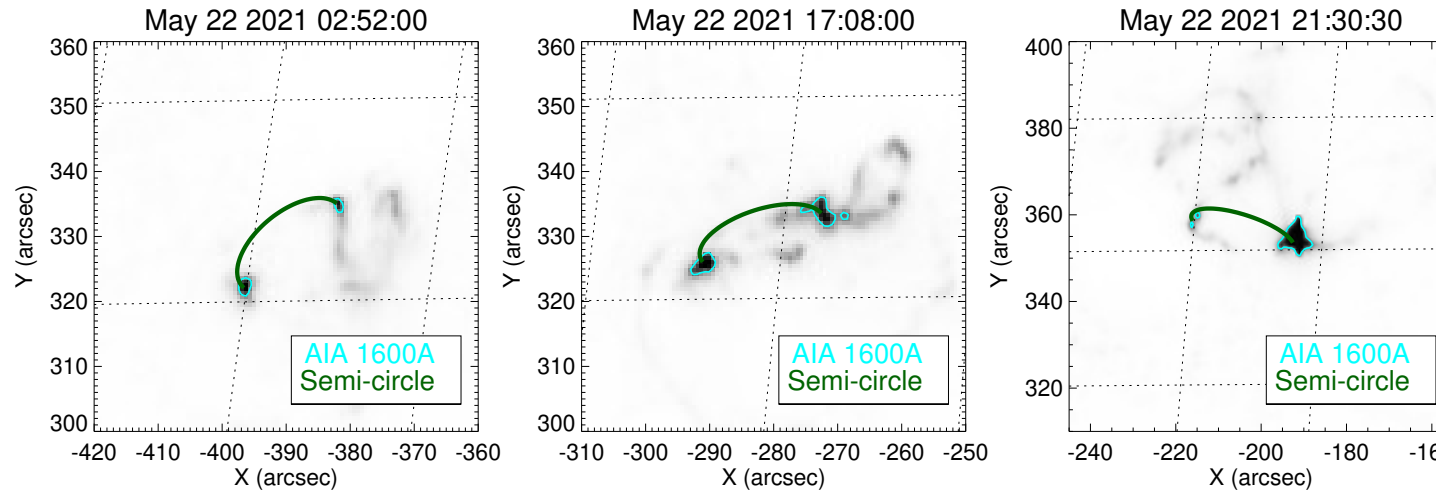


Shift front grid
→

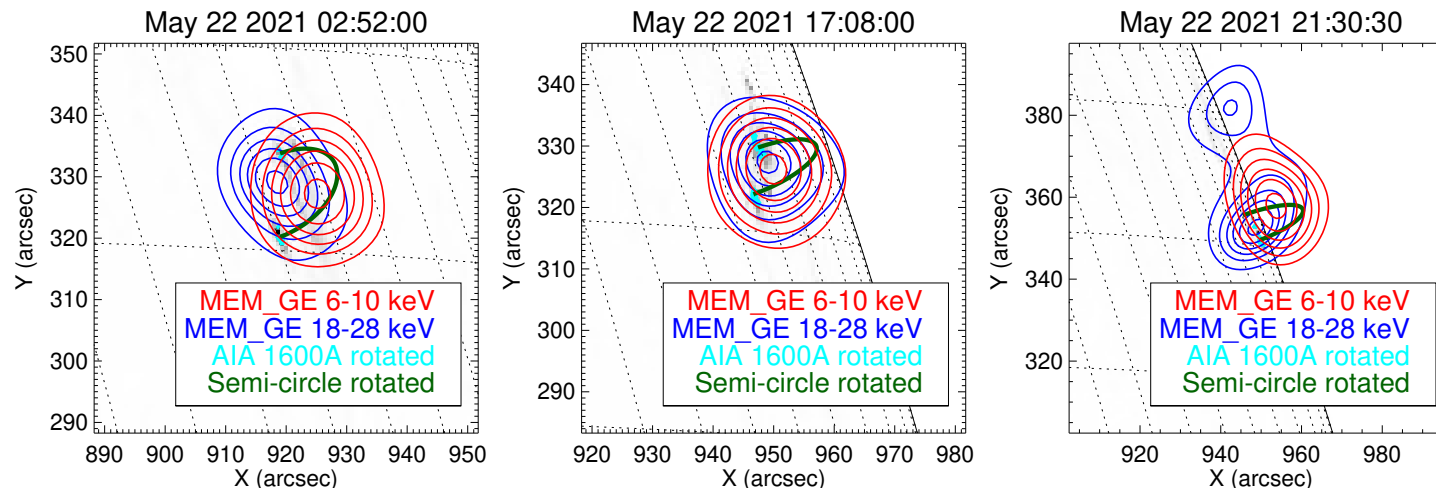


May 2021 events (Massa et al., 2022, in preparation)

Earth vantage point



Solar Orbiter vantage point



Active region AR2824

May 22:

- 02:52:00 UT: GOES C6.1
- 17:08:00 UT: GOES M1.1
- 21:30:30 UT: GOES M1.4

Manual shift STIX reconstructions

Event	Δx (arcsec)	Δy (arcsec)
02:52	47	55
17:08	47	50
21:30	50	50